MPHIL

3D Electrical impedance tomography using planar arrays

Wu, Quan Bao

Award date:
2018

Awarding institution:
University of Bath

University of Bath
Department of Electronic and Electrical Engineering

Thesis for Mphil Study in

3D Electrical impedance tomography using planar arrays

Student Name: Quanbao Wu
Supervisor: Professor. Manuchehr Soleimani
16/05/2018

List of symbols

B Magnetic flux density
$\nabla\cdot$ Divergence operator
$\nabla\times$ Curl operator
∇^2 denotes the Laplace operator
E Electric field
H Magnetic field
D Electric displacement vector
***L* Magnetic inductance**
J current density
μ Permeability
ε Permittivity
ε_0 is the electric constant
ρ is the total electric charge density (charge per unit volume).
ϕ Electrical potential
$\vec{n}$ The outward vector of the conductive domain
σ Conductivity distribution
j Current density
A Effective contact area of electrode
I_n The summation of current
V_n The summation of voltage
V_c Voltage drop across the contact impedance
Z_n Contact impedance
J Jacobian Matrix
J^T The transpose of Jacobian Matrix
J^{-1} The inverse of Jacobian Matrix
$\mathfrak{R}$ Tikhonov Matrix
λ Hyper-parameter
u Scalar potential distribution
n Outward unit normal of the boundary$\partial\Omega$
Z_l Contact impedance
I_l Injected current
U_l Corresponding potentials on the electrodes
L The number of electrodes
C_l The l-th electrode
Ω The closed domain of the object
(Ω) The associated Sobolev space which is an open subset of R^n
$\partial\Omega$ The smooth boundary of the object
$\mathfrak{R}$ Tikhonov Matrix
K constant
N constant
S constant
$|e_s|$ is the area of the s-th electrode.
A the area of the element
Z_{elec} assuming specified contact impedance
$[G]$ is the global matrix.
[V] is the potential matrix of nodes.
V_l is the potential value of each electrode.

Abstract

A Three dimensional (3D) electrical impedance tomography (EIT) planar array sensor is established for imaging detection. The advantages of a 3D planar array EIT are that they are low cost, mobile and of a non-invasive nature. The sensor is based on ~~the~~ impedance distribution within a closed domain. However, the inverse problem of EIT planar array is invasive and ill-conditioning. This means that a small error (noise or invalid data) ~~of~~ in the conductivity data can have a detrimental effect on the quality of reconstructed images. The Singular Value Decomposition is used to reduce noisy. In this report, a brief history of EIT and methodology are introduced. and an EIT model is described. In this research, a constant current is inputted and voltage readings are collected on a four-electrode-by-four-electrode array placed on the subsurface of the tank. An Electrical impedance and diffuse optical reconstruction software (EIDORS) project is used to reconstruct images by using electrical boundary measurements. Because of the general nonlinear and ill posed properties of EIT, a finite element forward model and algorithms of total variation are used to solve the forward and inverse problems respectively. In order to achieve a stable and fast image reconstruction process, a redundancy analysis method for EIT data is proposed. According to the redundancy analysis, the collected EIT data is divided into valid and invalid data. When the image is reconstructed from the useful data, singular value decomposition (SVD) is used to evaluate the effectiveness and the sensitivity map. The 3D images are reconstructed by the total variation regularization method. The results are shown by simulation and experimental tests. Through comparison of the reconstructed images of all the collected data and valid data, the quality of reconstructed images is not degraded, and the images reconstruction processing time can also be reduced.

Acknowledgements

This study was carried out in the Department of Electronic and Electrical Engineering at the University of Bath.

I wish to express my greatest gratitude to my supervisor Professor Manuchehr Soleimani. Without his support this thesis would have never been completed. I would also like to thank my group mates especially Mr. Bo Chen for many scientific and non-scientific discussions.

Contents

List of Tables

List of Figures

Figure 7.6 Reconstructed 3D simulation images of 4×4 planar array electrode EIT model of 4 positions (a) $\boldsymbol{x}$ =0; $\boldsymbol{y}$ =0; $\boldsymbol{z} = -20$cm(c) $\boldsymbol{x}$ =0; $\boldsymbol{y}$ =0; $\boldsymbol{z} = -30$cm (e) $\boldsymbol{x}$ =0; $\boldsymbol{y}$ =0; $\boldsymbol{z} = -40$cm (g) $\boldsymbol{x}$ =0; $\boldsymbol{y}$ =0; $\boldsymbol{z} = -50$cm; Reconstruction 3D experimental image of the 4×4 planar array electrode EIT model (b) $\boldsymbol{x}$ =0; $\boldsymbol{y}$ =0; $\boldsymbol{z} = -20$cm (d) $\boldsymbol{x}$ =0; $\boldsymbol{y}$ =0; $\boldsymbol{z} = -30$cm (f) $\boldsymbol{x}$ =0; $\boldsymbol{y}$ =0; $\boldsymbol{z} = -40$cm (h) $\boldsymbol{x}$ =0; $\boldsymbol{y}$ =0; $\boldsymbol{z} = -50$cm.

Figure 7.7 Reconstruction 3D simulation images of the 4×4 planar array electrode EIT model(a) upper right (c) bottom right (e) upper left (g) bottom left; Reconstruction 3D experiment images of the 4×4 planar array electrode EIT model(b) upper right (d) bottom right (f) upper left (h) bottom left.

Chapter 1: introduction

History

Electrical impedance tomography (EIT) has been developed intensively for more than 40 years, with the first published impedance image ~~was~~ presented by Henderson and Webster in 1976 [1, 2]. They designed and built an impedance camera with 100 electrodes to produce electrical impedance images of the thorax. It was the first time that the square array of surface-mounted electrodes was proposed. In 1983, Barber and Brown presented the first published impedance tomography images [2, 3]. They described a method of producing a tomographic image by using an electrical impedance tomography system with 16 electrodes. From 1986 to 1995, the European Union ~~has~~ successfully achieved Concerted Action on Impedance Tomography (CAIT) to stimulate European collaboration. And enormous progress has been made in EIT especially in clinical practice. Three dimensional images were proposed in order to improve the accuracy of the research [4].

Background

Electrical impedance tomography (EIT) is a technique and tool of imaging an impedance distribution within a closed domain, such as a cross section through a human body or other solid object using electrical sources[2, 5]. Compared with other advanced tomography techniques, such as CT, PET and MRI, Electrical impedance tomography techniques are non-intrusive, and ideally, non-invasive, portable, cost-saving, and release no radiation. Also, EIT technique can achieve rapid testing and long-term monitoring [2, 6]. EIT presents a spatial distribution (2D or 3D) of the impedance profile by a set of boundary data, of the injected current and measured voltage. The injection current is weak alternating current with amplitude between 1-5mA and frequency between 1-100 kHz, with the voltages being measured using the same electrodes. The conductivity distribution is calculated according to boundary voltage data. Moreover, the inverse problem is ill-posed proposed by Hadamard [16]. The 3D EIT reconstruction problem is an ill-posed inverse problem and algorithms are required to improve the image reconstruction technique[7]. Moreover, EIT has possibilities and improvements in visualizing the tissue physiology and pathology in terms of tomographic images of the electrical conductivity distribution, and hence it has been used in several applications, mainly in breast, lung and brain cancer [8].

Electrical impedance tomography by using 3D planar array provides a better option to detect industrial damaging compared with a traditional ring electrode testing system [9]. For some electrical impedance tomographic problems in areas of geophysics, archaeology, medical diagnosis and industrial plant control, the planar array is an appropriate electrode geometry [10]. For traditional EIT measurement with annulus electrodes, only 2D images can be obtained for each measurement. EIT by using 3D Planar Array can easily attach to the surface of objects and produces an 3D reconstructed structure within the tested domain. A constant current is injected, and voltages are collected on a four-electrode-by-four-electrode array placed on subsurface of the tank. Because of the general nonlinear and ill posed properties of EIT [11], finite element forward model and algorithms of total variation are used to solve the forward and inverse problem respectively. Tikhonov regularization based on L_2-norm and least square solution is one of the traditional method to solve the EIT inverse problem. However, it shows the blurred edges and boundaries of reconstructed images. To improve the quality of reconstructed images, the total variation regularization (TV) based on L_1-norm is used in this research to produce the reconstructed images.

Previous work has shown that systematic errors acquired can bring a serious affection during image reconstruction. Hence, the aim of the research is to investigate the effective method to reduce errors, effectively raise the measurement sensitivity and improve the resolution of reconstructed 3D EIT Planar array images. To achieve this aim, some small objectives and targets have been set below:

Objectives

1. Learn fundamental knowledge such as background, history, methods and applications.
2. Learn mathematical and physical theories such as forward model, inverse model, etc.
3. Learn how to use the lab hardware KHU Mark 2 and the EIT reconstruction software EIDORS, Netgen and Matlab to run the simulation program.
4. Building forward and solver models and applying simulation testing.
5. Comparing experimental testing with simulation testing.
6. Improve reconstruction algorithms.

Report Organization

This report has been divided into several chapters for showing clearly the ideas to readers. The history and background knowledge are introduced in the first chapter. The mathematical models and theories are explained in the second chapter. The hardware and software for EIT system are shown in the third chapter. And simulation and experimental analysis are illustrated in chapter four and chapter five respectively. Finally, potential future research and plans are discussed in the chapter six.

Conclusion

This chapter has given an overview of 3D Planar array Electrical impedance tomography (EIT) and the purposes of this research. The brief history of EIT is introduced and planar array EIT is proposed to detect objects with a closed domain. The fundamental knowledge of how 3D planar array EIT can be applied to industrial and clinical applications has been explained, and the benefits of planar array EIT has been illustrated. However, there are still many problems that need to be considered and solved such as the reconstruction algorithms to improve the quality of reconstructed images. And both software and hardware require improvement for future work. Therefore, this research is motivated to potentially contribute to improve the planar array EIT usage in industrial and clinical fields.

Chapter 2: theory

Mathematic models

The mathematical model used is the EIT model. The two parts of the EIT model are Forward problem and Inverse problem. The EIT model represents the relationship between the conductivity of all points within the closed domain and their corresponding potentials with a governing equation.
The forward solver solves the forward problem: 1. Solve the governing equation; 2. Compute the boundary voltage data by simulating a constant current within the closed domain in PC.

Maxwell's Equations

The electromagnetic field is induced by injecting current to electrodes which are governed by Maxwell's equations. These equations describe all (classical) electromagnetic phenomena.
In this work, a closed domain $\boldsymbol{\Omega}$ is given and the bounded subset of three-dimensional space with a smooth (or smooth enough) boundary $\partial\boldsymbol{\Omega}$ provided as well. The tested subject has a conductivity σ. The scalar potential is ϕ and the electric field is $E=-\nabla\phi$ which will be described in more detail later. The current density is $J=-\sigma\nabla\phi$, which is a continuum version of Ohm's law. In the absence of interior current sources, we have the continuum Kirchhoff's law $\nabla\cdot\sigma\nabla\phi=0$ [6].
There are three assumptions:

1. At low frequency (<100 KHz), displacement current is neglected.
2. Consider all testing objects as conductive.
3. The area of electrodes can be neglected.

The general field parameters in Maxwell's equations are the electric field *E* and the magnetic field *H.* These two parameters will be calculated as vector functions of space. It will be assumed that there is no relative motion in this work. The fields, when applied to a testing material or even vacuum, produce fluxes electric displacement *D* and magnetic flux *B*. The spatial variations of the fields and fluxes are derived from Faraday's Law of induction [6].

Faraday's Law describes that magnetic field B is produced by electromagnetic induction, which is given by [1],

$$\nabla\times\vec{\mathbf{E}}=-\frac{\partial\vec{\mathbf{B}}}{\partial t},\ \vec{\mathrm{E}}\text{ is electric field. (2.1)}$$

Ampere's law as induced by Maxwell to include the displacement current ∂D/∂t (Coulomb's law),

$$\nabla\times\vec{\mathbf{H}}=\frac{\partial\vec{\mathbf{D}}}{\partial t}+\vec{\mathbf{J}}\ (2.2)$$

where J is electric current density, D is electric displacement vector. And $\frac{\partial\vec{\mathbf{D}}}{\partial t}+\vec{\mathbf{J}}$ can be described as the free current density divided into two parts. Also $\frac{\partial D}{\partial t}$ is the current produced by the electric displacement vector, called displacement current. D is defined as [1]:

$$D=\varepsilon_0 E\ (2.3)$$

Where ε_0 is the electric constant.
Magnetic field B and H are related by the magnetic constant μ_0, the permeability, expressed as:

$$\mathbf{B}=\mu_0\mathbf{H}\ (2.4)$$

According to Gauss's laws for the electric field E and magnetic fields B, we have

$$\nabla\cdot\boldsymbol{E}=\frac{\rho}{\varepsilon_0}\ (2.5)$$

$$\nabla\cdot\mathbf{B}=0\ (2.6)$$

Because of the assumptions made, the electric field can be considered to be an electro quasi-static field. The properties of electro quasi-static field mean that the time-varying component can be ignored. Then the equations are:

$$\nabla \times E=0 \quad (2.7)$$

$$\vec{J}=\sigma \boldsymbol{E} \quad (2.12)$$

Where σ is the conductivity,

Combined $\nabla \times \vec{H}=\frac{\partial \vec{D}}{\partial t}+\vec{J}$(2.2) with $\mathbf{B}=\mu_0 \mathbf{H}$ (2. 4),

$$\nabla \times \vec{B}=\mu_0 \vec{J} \quad (2.8)$$

Also, the theorem of vector calculus which describes the divergence of a curl must always be zero. Hence,

$$\nabla \cdot \left(\nabla \times \vec{B}\right)=\nabla \cdot (\mu_0 \vec{J})=0 \quad (2.9)$$

Therefore,

$$\nabla \cdot \vec{J}=0 \quad (2.10)$$

Moreover, the Electric field is the minus value of the gradient of the electric potential.

$$E=-\nabla \phi \quad (2.11)$$

Combined $\vec{J}=\sigma \boldsymbol{E}$ (2.12) with $E=-\nabla \phi$ (2.11),

$$\nabla \cdot \vec{J}=\nabla \cdot (\sigma \nabla \phi)=0 \quad (2.13)$$

According to the divergence calculus,

$$\nabla \cdot (\sigma \nabla \phi)\ \nabla=\nabla \sigma \cdot \nabla \phi+\sigma \nabla^2 \phi=0 \quad (2.14)$$

Therefore,

$$\nabla^2 \phi=-\frac{\nabla \sigma \cdot \nabla \phi}{\sigma} \quad (2.15)$$

Conductivity σ and electric potential ϕ are two important parameters. The equation (2.15) describe the relationship between the forward model and inverse model. Forward model: given the conductivity σ, find electric potential ϕ. Inverse model: given the electric potential ϕ, find conductivity σ.

However, the image reconstruction of 3D planar array EIT is a nonlinear and ill-posed inverse problem based on the mathematical analysis. And it makes the image reconstruction to high-quality a challenging task. Using the iterative method the problem of Nonlinearity can be solved. Also, using regularization to obtain a stable solution can help to reduce the ill-posed inverse problem. There are several key factors to make ensure a high quality image, which are the performance of the forward solver, the measurement errors, the regularization technique, and the converging nature of the iterative algorithm [11, 12].

Boundary conditions

Boundary conditions are considered because Maxwell's Equations in integral form involve a closed domain. By giving the boundary conditions, a unique solution can be obtained. In Electrical impedance tomography (EIT), Neumann boundary conditions and Dirichlet boundary condition are two key types of boundary conditions which are required to solve problems.

To give more details, Electrical Impedance Tomography (EIT) is a non-invasive inverse method which is to determine the electrical conductivity σ of a medium within a closed domain Ω. In order to make voltage and current measurements at the boundary, related conditions and the mathematical model should be considered to solve problems.

Neumann boundary condition

Neumann boundary condition is used to get the solution on the boundary within a closed domain. There are two key equations, provided which are ordinary differential equations and partial differential equations. For solving the EIT forward problem, solution of the partial differential equation is required to be solved.

According to a partial differential equation, $\nabla^2 y(x) = 0$, where ∇^2 denotes the Laplace operator. The boundary condition taken on the boundary ∂Ω of the conductive domain Ω will be:

$$\frac{\partial y(x)}{\partial n} = \nabla y(x) \cdot \vec{n} \quad (2.16)$$

where $\vec{n}$ denotes the unit normal to the boundary ∂Ω and y is a given scalar function. $\nabla y(x)$ represents the gradient vector of $y(x)$.

Boundary conditions are complex because of the unknown current density *j*. But in most cases, *j* is considered as a continuous function. Therefore, the continuum model and gap model are proposed because of the advantage of being easy to calculate [13].

Electrode Model

There are four key types of Electrode modes which are described in details below. [11] The suitable electrode model of EIT is selected with the boundary conditions in order to obtain reasonable solutions for the forward problem.

Continuum Model

This model assumes that there are no electrodes provided and injected current I is a continuous function. For the experiments on the homogeneous tank, *j* is assumed to be $\sin k\theta$ or $\cos k\theta$. Therefore, the continuous function will be:

$$(\theta) = K\cos(N\theta) \quad (2.17)$$

Where K and N are constants.

The experimental studies show that in this model, the resistivities are overestimated because of the ignored electrodes' effects [29].

Gap Model

The gap model is better compared with the Continuum model. The gap model has S number of electrodes, and assumes that the injected current *j* is:

$$j = \begin{cases} \frac{I_1}{|e_s|} \ on\ e_s, s = 1, 2, \dots, S, (on\ the\ S^{th}\ electrode) \\ 0 \qquad off \quad \cup_{l=1}^{L} e_s \ , \qquad\qquad (on\ gaps) \end{cases} \quad (2.18)$$

where $|e_s|$ is the area of the electrode. The value of resistivity is overestimated by both the continuum model and the gap model. The shunting effect of the electrodes can be ignored. The shunting effect is produced by the contact with metal electrodes which provide a low-resistance path for the current.

Shunt model

In the Shunt model, because the electrodes are assumed to be perfect conductors, the potentials across the metal are considered as constant values.

$$\int_{e_s} \sigma \frac{\partial u}{\partial \vec{n}} \, dS = I_s, \ s = 1, 2, \dots, S \quad (2.19)$$

And

$$\sigma \frac{\partial u}{\partial \vec{n}} = 0 \quad off \ \bigcup_{s=1}^{S} e_s.$$

Because the potential on each electrode is constant,

$$u = U_s, \ s = 1, 2, \dots, S \quad (2.20)$$

However, the shunt model is not widely used because the resistances predicted are less than the experimental ones.

Conclusion

In this chapter, the brief mathematical models of electrical impedance tomography (EIT) has been introduced. It is clearly described that the relationship between electrical conductivity and magnetism in a closed domain are analysed and conducted by Maxwell's equations. But for simplicity, low frequency is assumed, and the magnetic field and electrode contact impedance can be neglected. Ohm's law is used to present the current density $\boldsymbol{J}$. The Kirchhoff's law is used to solve the interior current sources. The boundary conditions such as Dirichlet boundary condition are to determine the unique solution of boundary potential. And the Neumann boundary conditions which help to choose an earth point when determining boundary potential. The four electrode models which are used to help to get the forward solver are introduced briefly.

Chapter 3: EIT algorithms of Forward problem

The brief EIT forward model is shown below by Figure 3.1. According to the injected current data and conductivity distribution data which are based on the closed domain, the boundary voltages can be calculated.

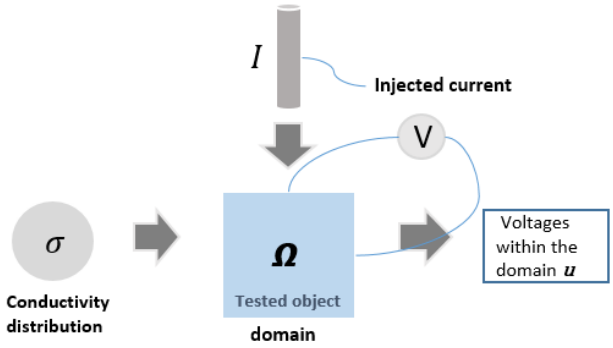

Figure 3.1 Forward model

Forward problem

In EIT, the electric field is described by the non-linear Laplace equation. And it is induced by the Maxwell equations and Ohm's law, and the Neumann boundary condition as shown below[14]:

$\nabla\cdot(\sigma\nabla u)=0$ (within the domain $\boldsymbol{\Omega}$) Laplace equation (3.1)

$u=\sigma(x, y)$ (on the domain $\boldsymbol{\Omega}$) Boundary condition (3.2)

$\sigma\frac{\partial u}{\partial \vec{n}} = \boldsymbol{j}(x, y)$ (on the domain $\boldsymbol{\Omega}$) Boundary condition (3.3)

$\boldsymbol{\sigma}$ is the electrical conductivity, u is the electrical potential, $\boldsymbol{\sigma}(x, y)$ is the boundary voltages and $\boldsymbol{j}(x, y)$ is the boundary current density.

The forward problem of the 3D Planar array EIT is to obtain the electrical potential from the conductivity distribution, which is to obtain u from $\boldsymbol{\sigma}$. The forward solver is to calculate node voltages within the domain by Laplace equations. Then the current density can be calculated by boundary conditions. And the forward solver is to help to get the inverse solver later. Maxwell's equations can be used for deeply understanding the forward model. For example, in a bounded two-dimensional system, the conductive domain Ω is given and its boundary is ∂Ω. Ω is a conductive material and its conductivity value is σ. And the forward problem is the whole process to compute its potential u on the boundary.
The interior current density j is produced by the electric field E:

$$j=\sigma E \quad (3.4)$$

Where σ is the conductivity. Because there is no internal current source within the domain Ω, the value of the interior current density should be zero. The electric field could be re-written as the minus value of the gradient of the electric potential u:

$$E=-\nabla u \quad (3.5)$$

The current density could be rewritten with the electric potential:

$$j = \sigma(-\nabla u) = 0 \quad (3.6)$$

The gradient of the density is zero:

$$\nabla\cdot(\sigma\nabla u) = 0 \quad (3.7)$$

To get the forward solver and compute the electrical potential, the boundary conditions are required. According to the Neumann boundary condition, the following function is:

$$\sigma\frac{\partial u}{\partial \vec{n}} = j \quad (3.8)$$

where,

$\vec{n}$ --the outward vector of the conductive domain
j – Current density
u -- Electrical potential

Boundary conditions are complex because of the unknown current density *j*. But in most cases, *j* is considered as a continuous function. Therefore, the continuum model and gap model are proposed because they are easily solved mathematically [13].

Finite element method

The finite element method is a numerical method which is used to obtain the electrical engineering numeric analysis in this research. In the EIT forward model, the finite element method (FEM) can obtain the approximation of the solution to u=σ (x, y). The analytical solution can be calculated by partial differential equations. The algebraic equations can be obtained by the finite element method formulation in a system. Therefore, the values of the unknown discrete number of points are estimated[1]. To solve the problem, it can be subdivided into smaller unit, simpler parts, which are known as finite elements.
In 2D EIT, the tested domain is divided into small elements such as triangles. The equations of small unit are integral to the whole system which models the entire problem.
In 3D EIT, the tested domain is divided into small elements such as polyhedral. And for each element the unknown value of potential is represented by a polynomial of a fixed order and the potential is assumed to be continuous[6].

Basic FEM formulation

In a typical network of electrical resistance, i and j are defined as typical resistance elements isolated from the whole system which is shown in the Figure 3.2. According to the Ohm's law, the current J_i and J_j can be defined as:

$$J_i = \frac{1}{r}(V_i - V_j) \quad (3.9)$$

$$J_j = \frac{1}{r}(V_j - V_i) \quad (3.10)$$

Rewritten in matrix form:

$$\begin{pmatrix} J_i \\ J_j \end{pmatrix} = \frac{1}{r}\begin{pmatrix} 1 & -1 \\ -1 & 1 \end{pmatrix}\begin{pmatrix} V_i \\ V_j \end{pmatrix} \quad (3.11)$$

Which can be written in a general form,

$$J = KV \quad (3.12)$$

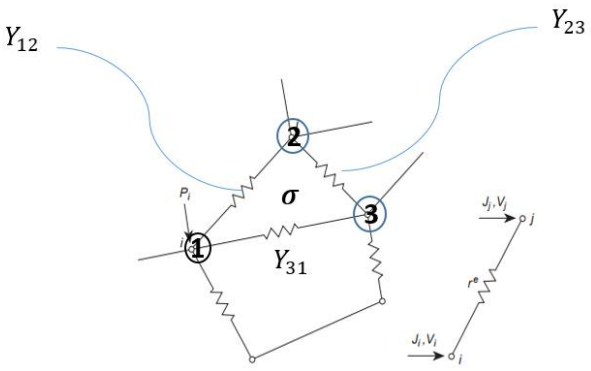

Figure 3.2 Finite element method equivalent circuit

It is easy to understand that the finite element method can be described as resistor networks in some simple electrical cases. In this 2D case, the conductivity σ is assumed constant on simplicity. To

determine the conductance of each edge by a resistor, $Y = \sigma\cot(\theta)$ is used to calculate. The angle θ_i is opposite the i-th edge. And the conductance $Y_i = \sigma\cot(\theta_i)$
For example, $Y_{23} = \sigma\cot(\theta_1)$
In the 3D case, the angle θ_i is between the two faces meeting at the edge opposite the i-th edge. And the conductance $Y_i = \sigma\cot(\theta_i)$
To give more details,
the coordinates for each node are (X_i, Y_i), i=1, 2, 3; The conductance between node i and j can be calculated by the equation $\boldsymbol{Y_{ij} = \frac{\sigma}{2A}\left(c_i c_j + d_i d_j\right), (i \neq j, i = 1,2,3; j = 1,2,3)}$ (3.13)
where σ is the conductivity constant value within the enclosed domain and A is the area of the element, i and j refer to the number of triangle nodes.

$$\boldsymbol{c_1 = y_2 - y_3 ; c_2 = y_3 - y_1 ; c_3 = y_1 - y_2 ;}$$
$$\boldsymbol{d_1 = x_3 - x_2 ; d_2 = x_1 - x_3 ; d_3 = x_2 - x_1 ;}$$

According to Kirchhoff's Law, YV=I, the node equation is provided below:

$$\begin{bmatrix} \boldsymbol{Y_{11}} & \boldsymbol{Y_{12}} & \boldsymbol{Y_{13}} \\ \boldsymbol{Y_{21}} & \boldsymbol{Y_{22}} & \boldsymbol{Y_{23}} \\ \boldsymbol{Y_{31}} & \boldsymbol{Y_{32}} & \boldsymbol{Y_{33}} \end{bmatrix} \begin{bmatrix} \mathbf{u_1} \\ \mathbf{u_2} \\ \mathbf{u_3} \end{bmatrix} = \begin{bmatrix} \boldsymbol{I_1} \\ \boldsymbol{I_2} \\ \boldsymbol{I_3} \end{bmatrix} \quad (3.14)$$

Where$\mathbf{Y_{11} = -Y_{12} - Y_{13}; Y_{22} = -Y_{21} - Y_{23}; Y_{33} = -Y_{31} - Y_{32}; Y_{ij} = Y_{ji}}$
In an EIT system, some adjacent elements might share the same resistor. In this case, the conductance value is equivalent with two different meshes generated resistors connected in parallel, which comes to:

$$\mathbf{Y' = Y_1 + Y_2} \quad (3.15)$$
$$\mathbf{Y_1 = \sigma_1 \cot \theta_1} \quad (3.16)$$
$$\mathbf{Y_2 = \sigma_2 \cot \theta_2} \quad (3.17)$$

$\mathbf{Y_1}$ is generated by element 1 with conductivity $\boldsymbol{\sigma}1$ and $\mathbf{Y_2}$ is related to element 2 with σ2, and $\mathbf{Y'}$is the value of the shared conductance. $\boldsymbol{\theta_1}$ and $\boldsymbol{\theta_2}$ are angles corresponding to the conductance Y' in element 1 and element 2.

Complete electrode model

The complete electrode forward model (CEM), which has been presented has the ability of modelling real-world electrode measurements reasonably well[13]. The assumptions are: 1) the boundary of the tested object Ω is smooth. 2) The boundary is partially covered with electrodes $e_s \subset \partial\Omega$, $1 \leq s \leq S$. All electrodes are identified and assumed to be ideal conductors. The Γ convergence of all electrodes is denoted by Γe = $U_s e_S \subset \partial\Omega$. Moreover, the current and voltage patterns are represented by I_s, $U_s \subset C$, $1 \leq s \leq S$, respectively.

$$u + Z_s\, \sigma \frac{\partial u}{\partial \vec{n}} = U_s \;\; on\; e_s, \;\; s = 1, 2, \ldots, S \quad (3.18)$$
$$\sigma \frac{\partial u}{\partial \vec{n}} = 0 \quad \text{on } \partial\Omega \backslash \cup_{s=1}^{S} e_s \quad (3.19)$$

To make the model even more flexible, it assumes that on Γn $\subset \partial\Omega$, Γn ∩ Γe = ∅, the current input is continuous; i.e., on Γn the data belongs to H˜ −1/2(Γn). Note that this type of Neumann boundary is not one of the formulations of the CEM; When conducting measurements with electrodes, a thin layer with high resistance is formed at the electrode interface[13]. It is specified by the contact impedance z : ∂Ω → C that this system is assumed to be an integral function.

Shape function

In FEM, the shape function is used to insert the solution between the discrete values obtained by the mesh nodes. The shape functions are able to find the nodal displacement at any point on the element. The conventional potential equation based on the EIT closed domain is expressed as:

$$\mathbf{v(x,y) = A + Bx + Cy=[1 \quad x \quad y]}\begin{bmatrix}\mathbf{A}\\ \mathbf{B}\\ \mathbf{C}\end{bmatrix} \text{ (3.20)}$$

In the EIT electrode system, electrodes are set on the boundary or plane of the domain Ω. According to the properties of FEM, the sum of all elements is required. The values of Elements are the areas of each electrodes, S is given. Assuming there are N electrodes with specified contact impedanceZ_{elec}, the function is given below:

$$\sum_{n=1}^{N}\int A\cdot\frac{1}{Z_{elec}}(V_n-u)dS$$

$$=\sum_{n=1}^{N}\frac{V_n}{Z_{elec}}\cdot\left(\sum_{j=1}^{3}\phi_j v_j\right)dS-\sum_{n=1}^{N}\frac{1}{Z_{elec}}\cdot\left(\sum_{j=1}^{3}\phi_j v_j\right)\cdot\left(\sum_{\mathrm{i}=1}^{3}\mathrm{u_i}\cdot\phi_{\mathrm{i}}\right) \text{ (3.21)}$$

Rewriting the function, finally, it will be given as below:

$$\sum_{n=1}^{N}V_l\sum_{j=1}^{3}v_j\int\frac{1}{Z_{elec}}\phi_j dS-\sum_{n=1}^{N}\sum_{i=3}^{3}u_i\sum_{j=1}^{3}v_j\int\frac{1}{Z_{elec}}(\phi_i\cdot\phi_j)dS$$

According to

LHS-RHS=0

Therefore,

$$\sum_{\mathbf{i}=1}^{3}\mathbf{u_i}\cdot\sum_{j=1}^{3}\int\boldsymbol{\sigma}\cdot\boldsymbol{\nabla}\boldsymbol{\phi_i}\cdot\boldsymbol{\nabla}\boldsymbol{\phi_j}\boldsymbol{d\Omega}\cdot-\sum_{n=1}^{N}\boldsymbol{V_n}\int\frac{\mathbf{1}}{\boldsymbol{Z_{elec}}}\boldsymbol{\phi_j}\boldsymbol{dS}+\sum_{n=1}^{N}\sum_{i=3}^{3}\boldsymbol{u_i}\int\frac{\mathbf{1}}{\boldsymbol{Z_{elec}}}\left(\boldsymbol{\phi_i}\cdot\boldsymbol{\phi_j}\right)\boldsymbol{dS}=\mathbf{0} \text{ (3.22)}$$

The current on all electrodes is the sum of the integral of the current density over the contact area in the whole system.

For each electrode, the current is given as:

$$I_n=\int\frac{1}{Z_{elec}}(V_n-u)\,dE_n$$

$$=\frac{V_n}{Z_{elec}}\int 1\,dE_n-\int\frac{1}{Z_{elec}}\cdot\sum_{\mathrm{i}=1}^{3}\mathrm{u_i}\cdot\phi_{\mathrm{i}}\,dE_n$$

$$=\frac{\boldsymbol{E_n}}{\boldsymbol{Z_{elec}}}\cdot\boldsymbol{V_n}-\frac{\mathbf{1}}{\boldsymbol{Z_{elec}}}\cdot\sum_{\mathbf{i}=1}^{3}\mathbf{u_i}\cdot\int\boldsymbol{\phi_i}\boldsymbol{dE_n} \text{ (3.23)}$$

Moreover, the forward problem is solved with a global matrix, which is:

$$[G]\cdot[V]=[I]$$

Where, $[G]$ is the global matrix. [V] is the potential matrix of nodes.

[V] is defined as the voltages matrix of all the nodes, each value of the nodes is u. V_l is the potential value of each electrode. The nodal potential matrix is given below:

$$[V]=\begin{matrix}u\\ V_n\end{matrix}$$

Assuming the matrix F which is given below:

$$\boldsymbol{F_{ij}}=\int\boldsymbol{\sigma}\cdot\boldsymbol{\nabla}\boldsymbol{\phi_i}\cdot\boldsymbol{\nabla}\boldsymbol{\phi_j}\boldsymbol{d\Omega}+\int\frac{\mathbf{1}}{\boldsymbol{Z_{elec}}}\left(\boldsymbol{\phi_i}\cdot\boldsymbol{\phi_j}\right)\boldsymbol{dS} \text{ (3.24)}$$

$$i=1,2\ldots K$$
$$j=1,2\ldots M$$

Also, assuming a matrix D which is given as below:

$$\boldsymbol{D_j}=-\int\frac{\mathbf{1}}{\boldsymbol{Z_{elec}}}\boldsymbol{\phi_j}\boldsymbol{dS} \text{(3.25)}$$

$$j=1,2\ldots M$$

Work out the matrix D' from current equations. A diagonal matrix Q is given as below:

$$\boldsymbol{D_i'}=-\int\boldsymbol{\phi_i}\boldsymbol{dE_n} \text{ (3.26)}$$

$$i=1,2\ldots K$$

And

$$\mathbf{Q} = \begin{bmatrix} \frac{\mathbf{E_n}}{\mathbf{Z_{elec}}} & \cdots & \mathbf{0} \\ \vdots & \ddots & \vdots \\ \mathbf{0} & \cdots & \frac{\mathbf{E_n}}{\mathbf{Z_{elec}}} \end{bmatrix} \quad (3.27)$$

So, the forward equation for the domain of interested with N nodes and L electrodes is:

$$\begin{bmatrix} F & D \\ D' & Q \end{bmatrix} \cdot \begin{matrix} \mathrm{u} \\ \mathrm{V_l} \end{matrix} = \begin{matrix} 0 \\ I \end{matrix} \quad (3.28)$$

Where in the nodal potential matrix [u], X elements are included which stand for N nodal voltage. Similarly, potentials of N electrodes are given by L elements in the matrix $[V_n]$.

$$[u] = \begin{bmatrix} u_1 \\ \vdots \\ \mathrm{u_X} \end{bmatrix}, [\boldsymbol{V_n}] = \begin{bmatrix} V_1 \\ \vdots \\ V_N \end{bmatrix} \quad (3.29)$$

The current vector and the null vector are given below:

$$[\boldsymbol{I}] = \begin{bmatrix} \mathrm{I}_1 \\ \vdots \\ \mathrm{I}_N \end{bmatrix}, [0] = \begin{bmatrix} 0 \\ \vdots \\ 0 \end{bmatrix} \quad (3.30)$$

Mesh generation

In EIT researches, mesh generation is used to clearly represent the surface shape of the region to be reconstructed into 2D or 3D images with all the geometry of the electrodes[15]. And in this research, mesh generated by NETGEN is very helpful. The electric field will be changed when the current stimulation pattern works. And it can be used to plot electrical potential distribution changes when inclusions are put into the closed domain.

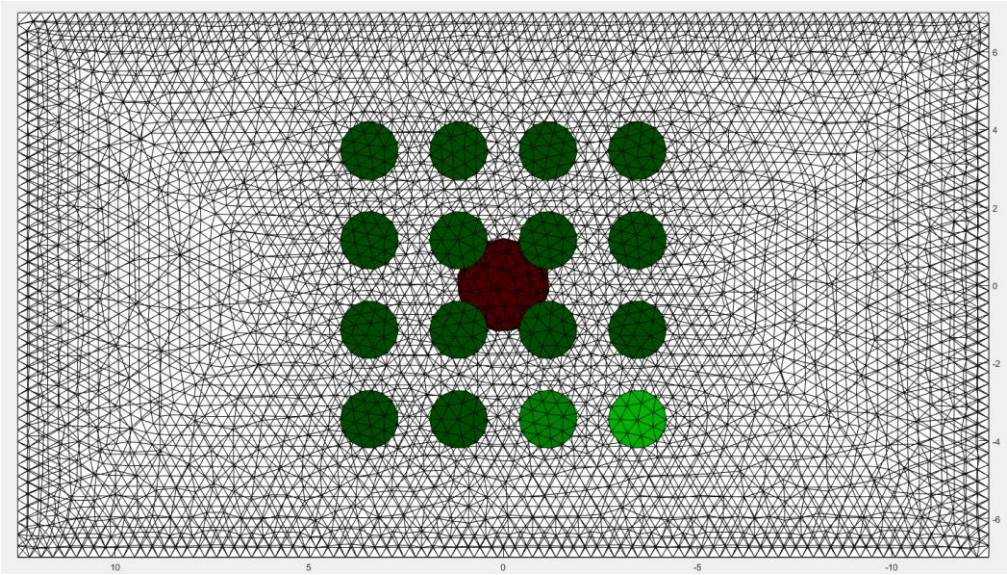

Figure 3.3 Top view of 3D planar array mesh generation with inclusion (metal ball)

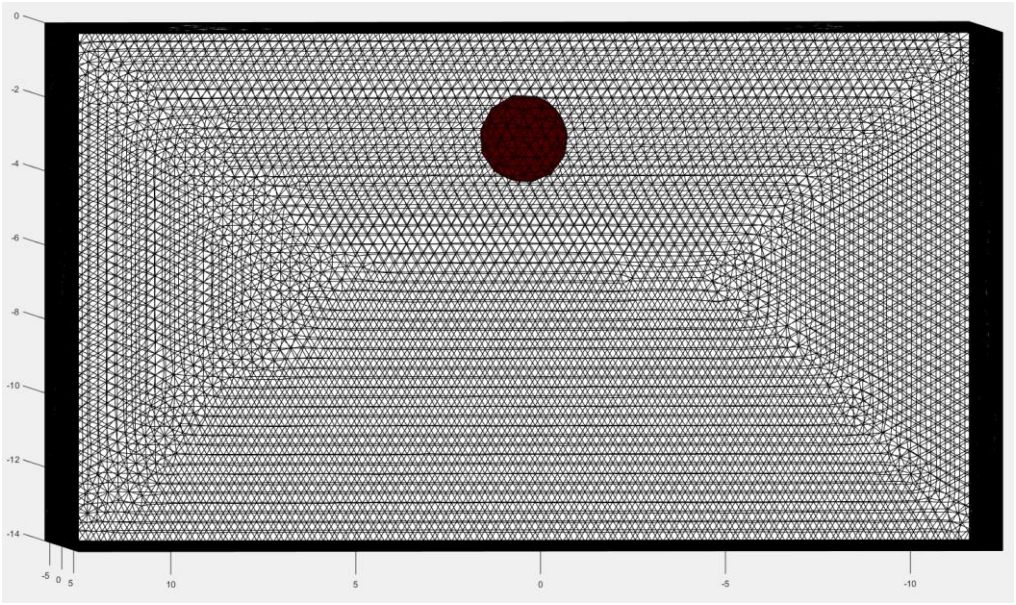

Figure 3.4 Front view of 3D planar array mesh generation with inclusion (metal ball)

Conclusion

In this chapter, the general forward problem is explained. The forward problem of the 3D Planar array EIT is used to obtain the electrical potential from the conductivity distribution, which is to obtain $\mathbf{u}$ from σ. And forward solver is used to predict (calculated) voltages according to the assumed conductivity (using existing mathematic models). Therefore, the calculated voltages can be compared to the measured data, and the error can be minimized. Also, the interior electric fields are required for the calculation of the Jacobian sensitivity matrix. Both the Finite Element Method (FEM) and Complete Element Method (CEM) are introduced for modelling the forward problem. And the Mesh generation is used to present the predicted voltages according to a function of conductivity.

Chapter 4: EIT algorithms of the Inverse problem

The brief overview of the EIT Inverse model is shown below in Figure 4.1. According to the injected current data and measured boundary voltage data which are based on the closed domain, the uniqueness of the solution of conductivity can be recovered.

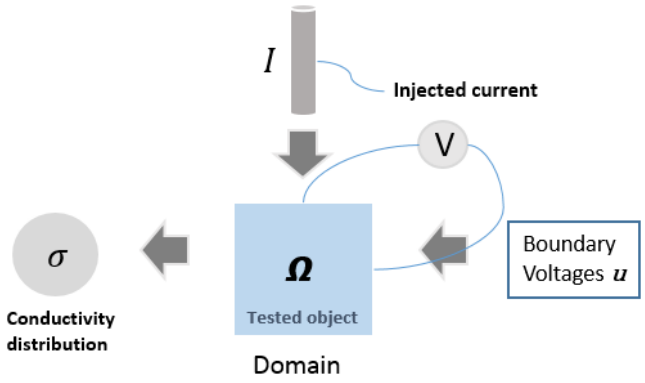

Figure 4.1 Inverse model

The inverse problem is ill-posed [16]. And for the direct problem which is well-posed, there are three key properties that need to be matched below:

1. There exists a solution to the problem
2. The solution is unique
3. The solution is stable

Mathematically, if a problem is unable to fulfil these three properties above, the problem is ill-posed and additional information is used to solve the inverse problem.
The inverse solver can solve the inverse problem by: 1. Minimizing the object function x_λ obtained from the voltage data both from the calculation and measurements. 2. Recovering conductivity or the uniqueness of solution.

Jacobian calculations

The Jacobian calculation is defined as vector $[J]$ for electrical conductivities [∇σ].
The standard Jacobian matrix is given as below:

$$[J] = \begin{bmatrix} \frac{\partial y_1}{\partial x_1} & \cdots & \frac{\partial y_1}{\partial x_k} \\ \vdots & \ddots & \vdots \\ \frac{\partial y_n}{\partial x_1} & \cdots & \frac{\partial y_n}{\partial x_k} \end{bmatrix} \quad (4.1)$$

Jacobian matrix is a matrix of all first order derivatives of a vector-valued function. Suppose $\mathrm{y}: R^n \rightarrow R^m$ is a function with input vector $\mathrm{x} \in R^n$ and $\mathrm{y(x)} \in R^m$. Then $[J]$ is $m \times n$ matrix.
So, for each of the elements of the Jacobian matrix, it is given as below,

$$J_{ij} = \frac{\partial y_i}{\partial x_j} \quad (i = 1,2,3,\dots,n)(j = 1,2,3,\dots,k) \quad (4.2)$$

For the inverse solution, the Jacobian matrix is defined as the potential difference over conductivity difference, which is represented as,

$$J_{ij} = \frac{\partial V_i}{\partial \sigma_j} \quad (4.3)$$

Where, i= 1, 2, 3… N, where B is the number of potential measurement, and j = 1, 2, 3… K, where K is the elements number of the FEM model.

Back-projection

Back-projection was used in the early EIT systems such as Sheffield Mark 1, and its inverse method can be used as a generalized Radon transform used in X-Ray CT, and early EIT[17].

The operator J^T of back-projection is followed by the application of the spatial filter$(J^T \mathrm{J} + \alpha^2 L^T \mathrm{L})^{-1}$. However, for the limitation of EIT conductivity distribution flow which is not the same as CT flow as it is not a neat beam, the reconstructed images are not defined. Although the volume of maximum sensitivity may be defined, the edges of the image are diffused. After being processed by the computer, the voltage differences will produce a blurred reconstructed image[15]. Therefore, a more developed algorithm is needed for more complication applications [18].

Sensitive Matrix Algorithm

In the sensitive matrix algorithm, the parameter J is defined as the difference of potential over the conductivity distribution which is the sensitive matrix factor as explained above. Therefore,

$$\Delta\Phi = \mathrm{J}\,\boldsymbol{\Delta} \quad (4.4)$$

Moreover, the inverse solver can compute the conductivity $\boldsymbol{\Delta\sigma}$ which is given as,

$$\boldsymbol{\Delta\sigma} = J^{-1}\Delta\Phi \quad (4.5)$$

Furthermore, because the weakness of the inverse problem which is ill- posed, the solution of the equation is non-unique. J^{-1} is given as

$$J^T\boldsymbol{\Delta\sigma} = J^{-1}.\, J^T\Delta\Phi \quad (4.6)$$

Rewritten with respect to the conductivity difference is as given below,

$$\Delta\sigma = (J^T J)^{-1}\,.\, J^T\,\Delta\Phi \quad (4.7)$$

Regularization

EIT usually involves the estimation of a large number of discrete conductivity values from a set of measurements of independent boundary voltage. The image reconstruction for EIT is mathematically a nonlinear and ill-posed inverse problem, regularization techniques were proposed as necessary for obtaining useful and stable solutions [19, 20]. The regularization usually involves prior information such as the differentiability of the function [21]. For the inverse problem, regularization parameters are able to adjust the estimated solutions.

In this work, Tikhonov regularization is used at the beginning, but the total variation regularization has been applied later because it preserves sharp discontinuities in images while removing noise and other unwanted details [19].

Hyper-parameter

The hyper-parameter is one of the regularizations used to avoid the instability of the system and to obtain the high resolution reconstructed images.

In addition, there is the L-curve, this is a log-log plot of the norm of a regularized solution[22]. For complex vectors $\mathbf{x} \in C^n$ and $\mathbf{b} \in C^m$and a complex matrix$\mathbf{A} \in C^{n\times m}$, x is required to be found for a given $\mathbf{Ax} = \mathbf{b}$. In EIT, $\mathbf{A}$ is the Jacobian while $\mathbf{x}$ will be a conductivity change and $\mathbf{b}$ a voltage error. The value of λ is a regularization parameter. When $\lambda \to 0$, x_λ is closed to the generalized solution.

$$x_\lambda = arg\min_x\{\|\mathbf{Ax} - \mathbf{b}\|^2 + \lambda^2\|\mathbf{Lx}\|^2\} \quad (4.8)$$

Associated with Tikhonov regularization below, it seems obvious that a good regularization parameter is one that relates to a regularized solution close to the L-curve 'corner'. This is because in this region

there is a good balance between achieving a small residual norm $\|\mathbf{Ax}-\mathbf{b}\|$and keeping the solution seminorm and $\|\mathbf{Lx}\|$reasonably small [23].

Singular value decomposition

According to the definition of singular value decomposition (SVD), SVD is the method of decomposing a matrix into three other matrices:

$$A = USV^T = \sum_{i=1}^{n} u_i \sigma_i v_i^T \quad (4.9)$$

Where:

- A is an $m \times n$ matrix
- U is an $m \times m$ orthogonal matrix, U=$(u_1, \dots, u_n)$
- S is an $m \times n$ diagonal matrix, S= diag$(\sigma_1, \dots, \sigma_n)$ has non-negative diagonal elements appearing in non-increasing order such as $\sigma_1 \geq \sigma_2 \geq \sigma_3, \dots, \geq \sigma_n$
- V is an $n \times n$ orthogonal matrix, V=$(v_1, \dots, v_n)$
- $U^T U = V^T V = I_n,\ m \geq n$

From the relations $A^T A = VS^2V^T$ and $AA^T = US^2U^T$, the SVD of A and the eigenvalue decompositions of the symmetric positive semi-definite matrices $A^T A$ and AA^T are strongly linked together[16]. This shows the uniqueness of the SVD of the given matrix A.

Because of its nature of being ill-posed, there are two characteristics of the SVD of A as shown below [16],

The singular values σ_i decay gradually to zero with no particular gap in the spectrum. An increase in the dimensions of A will increase the number of small singular values.

$$S = \begin{bmatrix} \sigma_1 & 0 & \cdots & 0 \\ 0 & \sigma_2 & \cdots & 0 \\ \vdots & \cdots & \ddots & \vdots \\ 0 & 0 & \cdots & \sigma_n \end{bmatrix}_{m \times n} \quad (4.10)$$

The left and right singular vectors u_i and $v_i$tend to have more sign changes in their elements as the index i increases, i.e., as σ_i decreases.

Obviously, the SVD is very useful for understanding the ill-conditioning of matrices, but it is more expensive to calculate large matrices.

In MATLAB, the command s=svd() is used to calculate the singular values. [U, S, V]=svd() is then used to calculate the singular value decomposition.

Tikhonov Regularization

One of the most well-known and useful regularization method is Tikhonov Regularization[24]. The background is assumed in basic linear algebra[6]. For complex vectors $\mathbf{x} \in C^n$ and $\mathbf{b} \in C^m$ and a complex matrix$\mathbf{A} \in C^{n \times m}$, x is required to be found for a given $\mathbf{Ax} = \mathbf{b}$. In EIT, $\mathbf{A}$ is the Jacobian while $\mathbf{x}$ will be a conductivity change and $\mathbf{b}$ a voltage error.

$$x_\lambda = arg \min_x \{\|\mathbf{Ax}-\mathbf{b}\|^2 + \lambda^2 \|\mathbf{Lx}\|^2\}$$

The value of λ is a regularization parameter. When $\lambda \to 0$, x_λ is closed to the generalized solution.

$$x_\lambda = (\mathbf{A}^T\mathbf{A} + \lambda^2 \mathrm{I})^{-1}\mathbf{A}^T\mathbf{b} \quad (4.11)$$

In this case, it should be

$$\Delta\sigma = (J^T\mathrm{J} + \alpha^2\mathrm{I})^{-1}.J^T\,\Delta u \quad (4.12)$$

I is the identity matrix.

Total variation regularization

The Total Variation (TV) regularization is a useful and important method for solving the inverse problem. It can produce sharp transitions in conductivity of the tested boundaries, and this leads to a more accurate estimated values and boundaries [25].

The total variation (TV) of a conductivity image is defined as:

$$TV\,(f) = \int_\Omega |\nabla f| d\Omega \quad (4.13)$$

Where Ω is the imaged region.

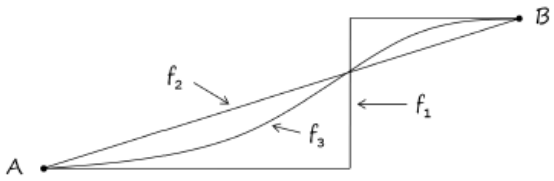

Figure 2.4 Points are connected by three different monotonically increasing functions with same TV.

As these are monotonically increasing functions with the same TV, the TV is:

$$TV\,(f) = \int_A^B f'(x)dx = f(B) - f(A) \quad (4.14)$$

For these 2D images, the TV of an image is the sum of the TV of each of the s edges, and it can be expressed as below:

$$TV\,(f) = \sum_s l_s \left| f_{m(s)} - f_{n(s)} \right| \quad (4.15)$$

Where l_s is the length of the s^{th} edge in the mesh, $m(s)$ and $n(s)$ are the indices of the two opposite elements of the s^{th} edge, and the index s is the range of all the edges. It can be expressed as[26]:

$$TV\,(f) = \sum_s |L_S f| \quad (4.16)$$

Where L is a sparse matrix, and $m(s)$ and $n(s)$ are non-zero values in L_S= [0, ..., 0, l_s , 0, ..., 0, $-l_s$, 0...0] .

Image quality assessment

The quality of reconstructed images is the key factor which is be considered for further developments. And the resolution of EIT is lower than that of CT or MRI because of its ill-conditioned problems. But

the quality has been improved greatly in the last few years. The quality can be assessed by the following factors: Resolution (RES), Shape Deformation (SD), Amplitude Response (AR), Position Error (PE), Noise Amplification (NF) and Ringing Effect (RNG) [27].

Resolution (RES)

The resolution (RES) measures the size ratio of reconstructed targets to the whole reconstructed area. It can be expressed as below:

$$RES = \sqrt{\frac{A_q}{A_0}} \quad (4.17)$$

$$A_q = \sum_k [\widehat{X_q}]_k \quad (4.18)$$

where A_q is the number of pixels in $\widehat{Xq}$, and A_0 is the area (in pixels) of the entire reconstructed medium. The square root is used to measure the areas ratio instead of radius ratio.

EIT is currently considered a low resolution medium which means a non-uniform RES can produce an incorrectly reconstructed position of a larger object. RES requires high resolution and it should be uniform and small. Therefore, RES is less important to be applied.

Shape Deformation (SD)

The shape deformation (SD) measures the fraction of the unfit ¼ amplitude set of reconstructed targets. It can be expressed as below:

$$SD = \frac{\sum_{k \notin C} [\widehat{X_q}]_k}{\sum_k [\widehat{X_q}]_k} \quad (4.19)$$

Where C is a circle centred at the C_0G of $\widehat{Xq}$ with a n equivalent area to A_q [27]. For producing high quality reconstructed images, SD should be low and uniform. Therefore, it is less important.

Amplitude Response (AR)

The amplitude response (AR) measures the ratio of the amplitudes of the simulated image pixel to that of the total image pixel. It can be expressed as below:

$$AR = \frac{\sum_k [\widehat{X}]_k}{V_t \frac{\Delta\sigma}{\sigma_r}} \quad (4.20)$$

Where,
V_t is the volume of the image target on the electrode plane
σ_r is the reference conductivity distribution
$\Delta\sigma$ is the differences between real conductivity and reference conductivity
AR is required to be constant as it is the key factor for producing correct images

Position Error (PE)

The position error (PE) measures the position of the image target. It can be expressed as below:

$$PE = r_t - r_q \quad (4.21)$$

Where,
r_t is the real position of the image target
r_q is the centre of gravity (C_0G) of $\widehat{Xq}$
For producing good quality and reliable images, PE should be small and constant.

Noise Amplification (NF)

The noise amplification (NF) is the ratio of the output signal to input signal to noise ratio (SNR) which measures the noise level of image amplitude instead of image energy.
SNR can be expressed as below:

$$SNR = \frac{mean|signal|}{std\ noise} \quad (4.22)$$

NF can be expressed as below:

$$NF = \frac{\frac{E[mean|\widehat{Xt}|]}{E[std\widehat{Xn}]}}{\frac{E[mean|y_t|]}{E[stdy_n]}} \quad (4.23)$$

For regulation algorithms, the value of NF is determined by the hyperparameter selection. And NF should be low and can be ideally used in EIT hardware. For Sheffield backprojection. NF=0.5 has generally been considered to be satisfactory. Therefore, low NF (0.5) can be considered to be applied in EIT systems.

Ringing Effect (RNG)

The Ringing Effect (RNG) measures the ratios of the image amplitude of the opposite sign surrounding areas to that of the main reconstructed target area. It can be expressed as below:

$$RNG = \frac{\sum_{k\notin C\ \&\ [\widehat{X}]_{k<0}}[\widehat{X}]_k}{\sum_{k\in C}[\widehat{X}]_k} \quad (4.24)$$

RNG should be uniform and low for producing high quality reconstructed images. Overshoot could lead to incorrect interpretation of the images.

Conclusion

In this chapter, the inverse problem and inverse solver are briefly explained. For solving the inverse problem, Jacobian calculations, regularizations, and singular value decomposition are introduced clearly. The Jacobian matrix is used to calculate the partial derivatives of voltages with respect to conductivity parameters. Moreover, regularizing EIT is proposed because of the ill-conditioning problem of inverse problem. Total variation regularization is used to improve the numerical efficiency and stability, also the poor quality of reconstructed images can be improved in this way. The K-th derivatives numerically in singular value decomposition illustrate the redundancy analysis of planar array EIT.

Chapter 5: Hardware and software of EIT system

Electrical impedance tomography (EIT) aims to reconstruct the image of a conductivity distribution within the testing object. EIT systems measure boundary voltages according to constant, low frequency and multiple injection currents to reconstruct cross-sectional images of the conductivity distribution [28].

EIT System

All the proposed EIT systems are based on the basic methodology which are: 1) the data collection of a set of independent transfer electrical impedances. 2) The stable solutions of forward and inverse problems in order to reconstruct images of a high quality [2].

To reconstruct EIT images based on general geometrical properties, all functions are required which are described in detail: a system for measuring the surface structure, a mesh generator to produce a mesh based on the surface information, code for computing the finite element approximation and an algorithm to solve the inverse problem. Also, tools to display the results and also to analyse the images are required [29]. Therefore, 4 key parts of the EIT system are shown below in Figure 5.1:
The basic EIT system has four main components:

① EIT-hardware system (instrumentation)
② 3D Electrode Array or EIT Sensors (in this research, it is 3D Electrode planar array)
③ Computer system with Reconstruction Algorithms
④ Object under test (OUT)

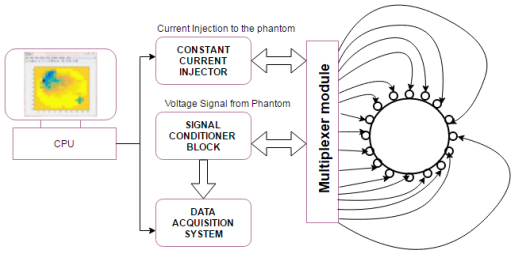

Figure 5.1: General EIT system structure

KHU Mark2 is a parallel multi-frequency EIT system and it is operated by the impedance measurement module (IMM). In the KHU Mark2 system, a constant current source and a voltmeter are included in the system. FPGA works with a main controller which is independently in the IMM system. The KHU Mark2 can provide between 1 and 64 channels. In the research, the KHU Mark2 is assembled with 16 channels [6].

System structure

The KHU Mark2 EIT system is the EIT-Instrumentation mentioned above. And it is applied for both 3D-EIT and 2D-EIT systems. In this, research, it is tested with a 3D EIT system. The KHU Mark2 EIT system is comprised of five main parts: (i) a computer with a USB port and EIT software (ii) a main controller, DSP (TMS320LF2812A, Texas Instruments, USA) with a USB interface, (iii) an intra-network controller on a digital backplane, (iv) impedance measurement modules (IMM) and (v) switching circuits on an analogue backplane. Figure5.2 shows its structure.

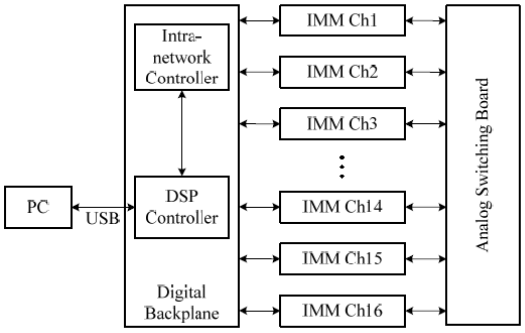

Figure 5.2 Structure of the KHU Mark2.

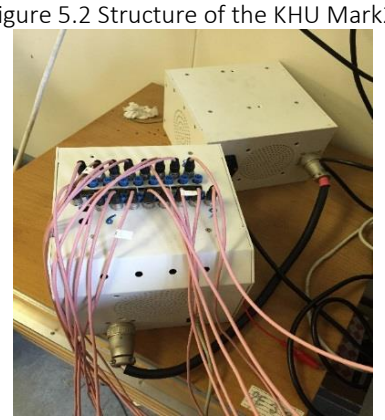

Figure 5.3 The main body of the KHU Mark2.

By using 16 IMMs, a 16-channel KHU Mark2 EIT system is used to test in this research. Because IMMs are independent in the system, the KHU Mark2 is able to inject current and measure voltage in any possible combination at the same time. Also, 4 generalized impedance converters (GIC) are used to cancel out stray capacitances at frequencies above 10 kHz. Using a high-capacity FPGA (EP3C10F256C8N, Altera, USA), the IMM performs all necessary functions including digital waveform generation, phase-sensitive demodulation, data exchange and controls [28].

EIT system development

There are 5 versions of EIT hardware system. And these systems are from Sheffield University research group, Oxford University research group and Kyung Hee University group separately. The data acquisition protocol for these systems is the neighbouring method [28, 30, 31].

The developments of EIT systems are shown below. The data acquisition speeds have been increased, and the mechanical design of these system have become more compact as well as the frequency range increasing. For the Sheffield system, the voltages are collected from electrodes which are not used for current injection, this is to minimize the effects of unknown electrode skin contact impedances. For KHU EIT systems, it measures voltages and currents on all electrodes [31]. A current source is included in the KHU Mark 1 system. And a switching circuit is used to inject current between a chosen pair of electrodes sequentially. Although there are multiple independent voltmeters in this system, two inputs of each voltmeter are connected to an adjacent pair of electrodes and to help to overcome these limitations, the KHU Mark2 was developed [28, 32-34]. For the Oxford EIT system, the uniqueness of OXPACT-II is the voltage drive and current measurement architecture. High-quality programmable voltage sources are easier to achieve than current sources and have been used to deliver currents in an EIT application [35, 36]. OXBACT-III is a real-time multiple-drive adaptive system, and it is used to operate at several frequencies and is based on the adaptive current method [37].

Identified EIT system	Date	Electrodes	Current driven pattern	Frequencies	Technology	Current source
MK1	1987	16	adjacent drive/receive	50 KHz	Analogue	single
Space/portable	1989	16	adjacent drive/receive	50 KHz	Analogue	single
MK2	1990	16	adjacent drive/receive	20KHz	Digital	single
MK3	1993	16	Interlaced	8:9.6KHz-1.2MHz	Analogue	single
MK3.5	2000	8	adjacent drive/receive	30:2KHz-1.6MHz	Digital	single

Table 5.1: Developments of EIT systems in Sheffield [30]

Oxford EIT system	Date	Electrodes	Frequency	Current source
OXPACT -II	1991	32	9.6KHz	Multiple current source
OXBACT-III	1994		10-160KHz	Multiple current source

Table 5.2: Oxford EIT system development

Kyung Hee EIT system	Electrodes	Frequency
KHU Mark I	16/32/64	10HKz-500HKz
KHU Mark II	16/32/40	10Hz-1MHz

Table 5.3: KHU EIT system development

Software

The Electrical Impedance and Diffuse Optical Reconstruction Software project (EIDORS) aims to develop freely available software that can be used to reconstruct electrical or optical material properties from boundary measurements [38]. In this project, EIDORS is used for reconstructing electrical impedance images in three dimensions.

For the Nonlinear and ill-posed problems, a finite element model is typically used to process the forward solution. And for obtaining a unique and stable inverse solution, a regularized nonlinear solver is used. However, those finite element programs for commercial business are not suitable for solving these problems because of the lack of calculating the Jacobian and accurate electrode modelling. Moreover, most industrial and medical electrical imaging problems are applied to three-dimensional. To meet more requirements, EIDORS was developed and released to solve the forward and inverse problems of EIT in three dimensions based on the complete electrode model along with some basic visualization utilities. Also, the formulation induced by the Jacobian (or sensitivity) matrix based on the complete electrode model is included [39].

The software used in the EIT system is KHU-Mark 2. KHU-Mark 2 provides functions such as the data acquisition and real-time images reconstruction. It produces real-time images in 4 steps and figures of which are shown below. The 4 steps of operating KHU-Mark 2 are: connect check button, select 10 KHz as frequency setting, data saving to a specified file path and scan data with a set of 204 measured values.

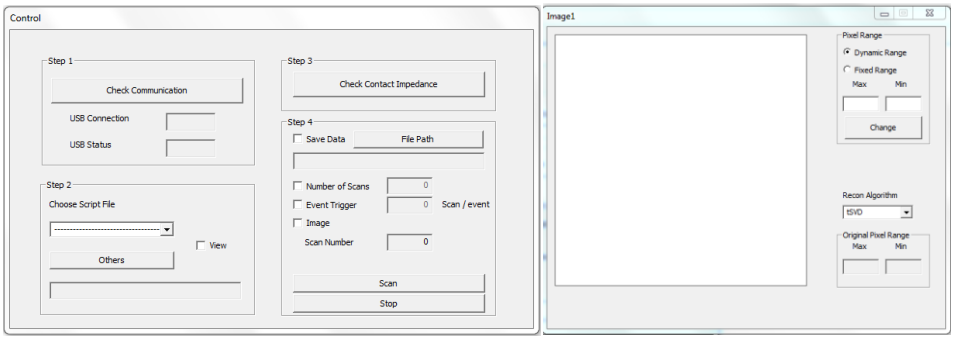

Figure 5.4: 4-step setting and image window in system

Theory of EIDORS

Brief introduction

The EIDORS (electrical impedance and diffuse optical reconstruction software) project aims to build a PC software system to produce reconstructed images from electrical or diffuse optical data [40]. MATLAB can be used in the EIDORS system for the functions of rapid prototyping, graphical user interface construction and image display. In this work, EIDORS, MATLAB and NETGEN can be used for three-dimensional mesh generation, solving the forward problem, getting the stable inverse solutions and reconstructing tomographic images.

Meshing

For solving the boundary value problems, the finite element uses the complete electrode model to compute approximate solutions involving models with first-order tetrahedral elements[38].
Many mesh generators are available and easily imported in Matlab. And it could be used in medical EIT and industrial EIT. For example, the representation of mesh generators are quality mesh generation (QMG) [41], Netgen [42, 43]and FEMLAB [44]. EIDORS can use Netgen to create sophisticated 2D and 3D models. In this work, EIDORS is used to create the 3D subsurface EIT model.
Although there are challenges in EIT research, much progress has been made of late. In this work, Netgen is used as an advanced 3D-mesh generator which automatically produces a 3D tetrahedral mesh. The mesh is properly presented with the measured voltages as a function of conductivity to a high accuracy. Netgen provides a data structure to represent the geometry of the closed domain to be meshed. This includes the external boundary shape, internal structures and surface attached by electrodes[6].
The structure of the NETGEN mesh process is shown below:

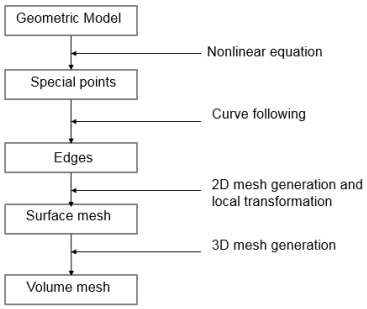

Figure 5.5: structure in mesh generation

EIDORS structure

EIDORS software consists of four main components: data, image, forward model (*fwd_model*) and inverse model (*inv_model*). Each component is represented by a structure. All components have the properties of a name and type [45].

fwd_model: Forward model is proposed to represent the finite-element model (FEM), phantom shape, electrode shapes, positions and properties. Also, the current stimulation patterns and voltages measured patterns are included.

inv_model: Inverse model is used to represent the reconstruction information including regularized images.

Calculation of the Jacobian: the most complex and important part is the Jacobian calculation. The Jacobian matrix is also called the sensitivity matrix **J**. The Jacobian calculation is the matrix of first order derivatives of voltages with respect to conductivity parameters [6, 45].

Jacobian (V, σ) computes the Jacobian matrix of Voltages (V) with respect to conductivity (σ).

J = calc_jacobian (fwd_model, img)

$$J_{i,j} = \frac{M_i V_{meas} \partial F(\sigma, I_i)}{\partial \sigma_j} \Big|_{\sigma=\sigma_0} \quad (5.1)$$

Where ***F*** is the FEM model of an EIT medium, $\boldsymbol{\sigma}$ is the vector of electrical conductivities and ***I*** is the current stimulation pattern. The measured voltages can be represented as a linear combination of voltages, V_{meas}. For each simulation pattern, I_i, a vector of measurements M_i is acquired, each of which consists of a linear combination of electrode measurements, represented by M_i . Thus, where σ_0 is the 'background' conductivity around which small changes are assumed to occur. To represent $J_{i,j}$ as a matrix, measurements for all stimulation patterns i are flattened into column vectors which are concatenated for each finite element j. In EIDORS, the Jacobian is calculated using the function calc_jacobian, which takes as parameters the FEM model (type fwd_model) and the image of σ_0 (type image) [45].

Data collection methods

Three data collection methods which are the neighbouring, the cross, and the opposite methods are commonly considered in EIT[46]. The difference between those three methods is the drive pattern of current injection and voltage collection. Also, the accuracy is increased by using a pair drive EIT system compared with a multiply drive EIT system [12, 47]. In this project, only a pair drive is used to run the system.

The neighbouring method

The Neighbouring Method is also known as the adjacent drive method [2]. In this method, the current is injected in a pair of adjacent electrodes and the voltages are measured separately from all other adjacent electrode pairs. Figure 5.6 and 5.7 below show the neighbouring method for a 16-eletrode EIT planar array system. In Figure 5.6, the current is applied with electrode 1 and electrode 2. Moreover, the voltages are measured separately from electrode pairs 3-4, 4-5, ..., to 15-16. Therefore, the 13 voltages data are collected. In Figure 5.7, the current is injected into electrode 2 and electrode 3. Then another 13 voltage data collection process repeats until the current is applied with electrode 16 and electrode 1, which means that a 16-electrode system would produce 208 measurement outputs(N*(N-3)/2=16*13=208).

For the neighbouring method, the current density is highest in the injecting electrode pair. Also, the current density decreases rapidly with the increase of distance between the injecting electrode pair and the rest electrodes. Therefore, this method is more sensitive to conductivity close to the boundary compared with the central part. The resolution is greater on the outer regions and relatively lower in the centre region. Furthermore, it is sensitive to perturbations in the boundary shape of the object, in the positioning of the electrodes and is quite sensitive to measurement error and noise [2].

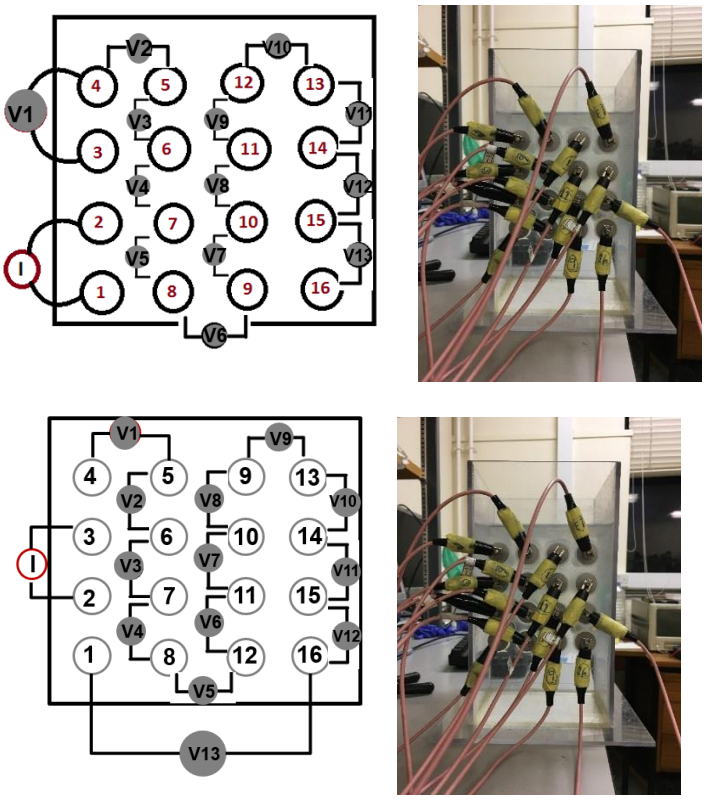

Figures 5.6 and 5.7: The Neighbouring method: Diagram (left) and experiment (right)

The Cross Method

The cross method which is now rarely used in EIT data collection compared to the neighbouring method, because it has low sensitivity in the periphery and it is more sensitive over the entire region [5]. Figures 5.8 and 5.9 below show the cross method for a 16-electrode EIT planar array system. In the cross method, adjacent electrodes are chosen as current and voltage references separately. As figures 5.8 illustrates below, the current is applied with electrode 16 and electrode 2. Moreover, the voltages are measured sequentially from electrode pairs 1-3, 1-4, ..., to 1-15. Therefore, the 13 voltages data are collected. To give more details, the electrode 1 is selected as voltage reference against the other 13 electrodes and electrode 16 is the current reference electrode. Furthermore, figures.5.9 shows the repeated procedure when the current is applied to electrode 16 and electrode 4. Another 13 voltage measurements are taken by using electrode 1 as a reference electrode. The entire procedure is repeated until current is applied to electrode 16 and electrode 14 with electrode 2 and electrode 3 as reference electrodes separately. Therefore, 91 (7*19=91) measurements are collected.

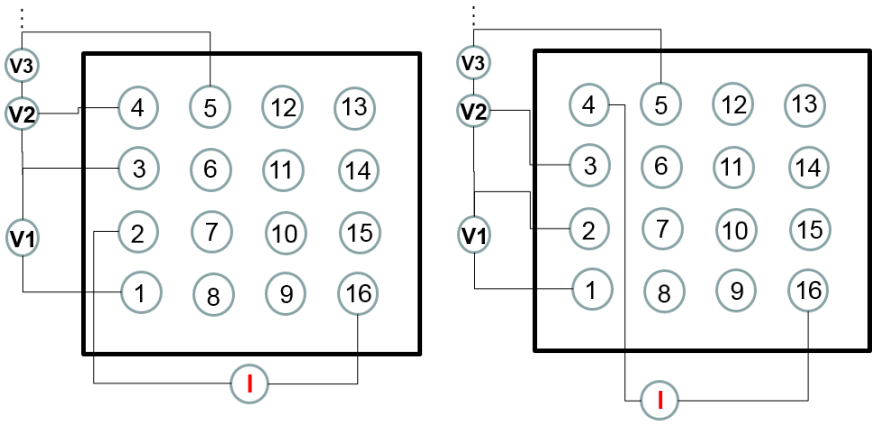

Figures 5.8 and 5.9: The Cross method

The opposite method

The opposite method which was proposed by Hua et al is commonly used in EIT the brain area [3], because it is less sensitive to conductivity changes at the boundary [2]. In this method, current is applied with electrodes which are 180 degrees apart with the voltage measurements of the remaining electrodes. Figure 5.10 below shows the opposite method for a 16-electrode system. As figures 5.10 illustrates below, the current is injected in electrode 1 and electrode 13, and the voltages are measured sequentially from electrode pairs 2-3, 2-4, ..., to 2-15. Therefore, the 13 voltage data are collected. Moreover, electrode 2 is selected as voltage reference against the other 13 electrodes. The entire procedure is repeated until current is applied to electrode 16 and electrode 8. Therefore, 104 (8*13=104) measurements are collected. For the opposite method, the current distribution is more uniform and has a good sensitivity and distribution [18].

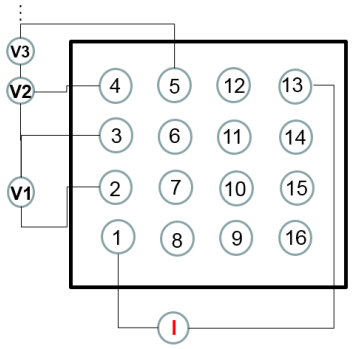

Figures 5.10: The opposite method

Conclusion

In this chapter, the hardware and software of the EIT system are introduced. For the hardware EIT system, KHU Mark 2 is mainly explained, and for the software EIT system, MATLAB and NETGEN are illustrated clearly. The data acquisition method which is also known as current stimulation patterns are briefly described. In this research, the neighbouring data collection method is used as its conductivity is more sensitive to the boundary domain.

Chapter 6: Simulation Tests

Before the experimental test, the simulation tests were done to test the feasibility and performance of the planar array model. EIDORS and Netgen were used to reconstruct 3D images. The purposes of the 3D planar array simulation test are:

- To show the possibilities of detecting objects
- To show the quality of 3D image reconstruction
- To show the possibilities of the depth ranges of objects
- To compare the original reconstructed images with the reconstructed images after redundancy analysis.

Modelling

The methods of building the forward model, forward solver, inverse model and inverse solver are described in Chapter 4 and 5 above. The finite element method (FEM) is used to piecewiselly discretize the 3D region into small voxels. In the forward model, the current pattern is selected as a neighbouring stimulation, and the conductivity distribution is pre-defined. The sensitivity matrix which is also known as a Jacobian Matrix is determined by voltage differences. When finishing modelling the forward model, algorithms are applied to calculate the actual conductivity distribution with the measured voltages. The accuracy of the system is determined both by the forward and inverse model.

Simulation test 1

In simulation test 1, a metal ball with $r = 0.5$ is put on the 4 positions close to the surface of the phantom.

Positions	**Simulation model**	**Reconstructed images**
$\boldsymbol{x}$ **=1.7** $\boldsymbol{y}$ **=1.7** $\boldsymbol{z}$ **= −1.2**	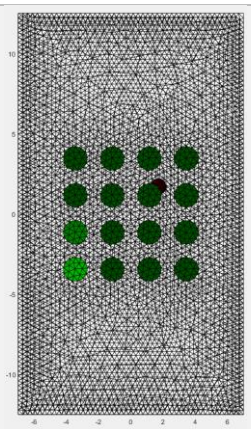 (a)	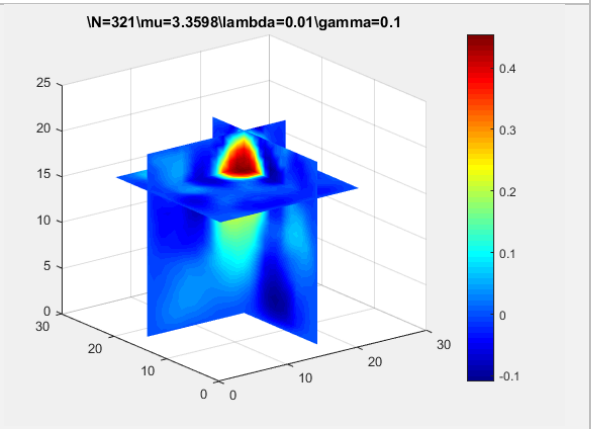 (b)

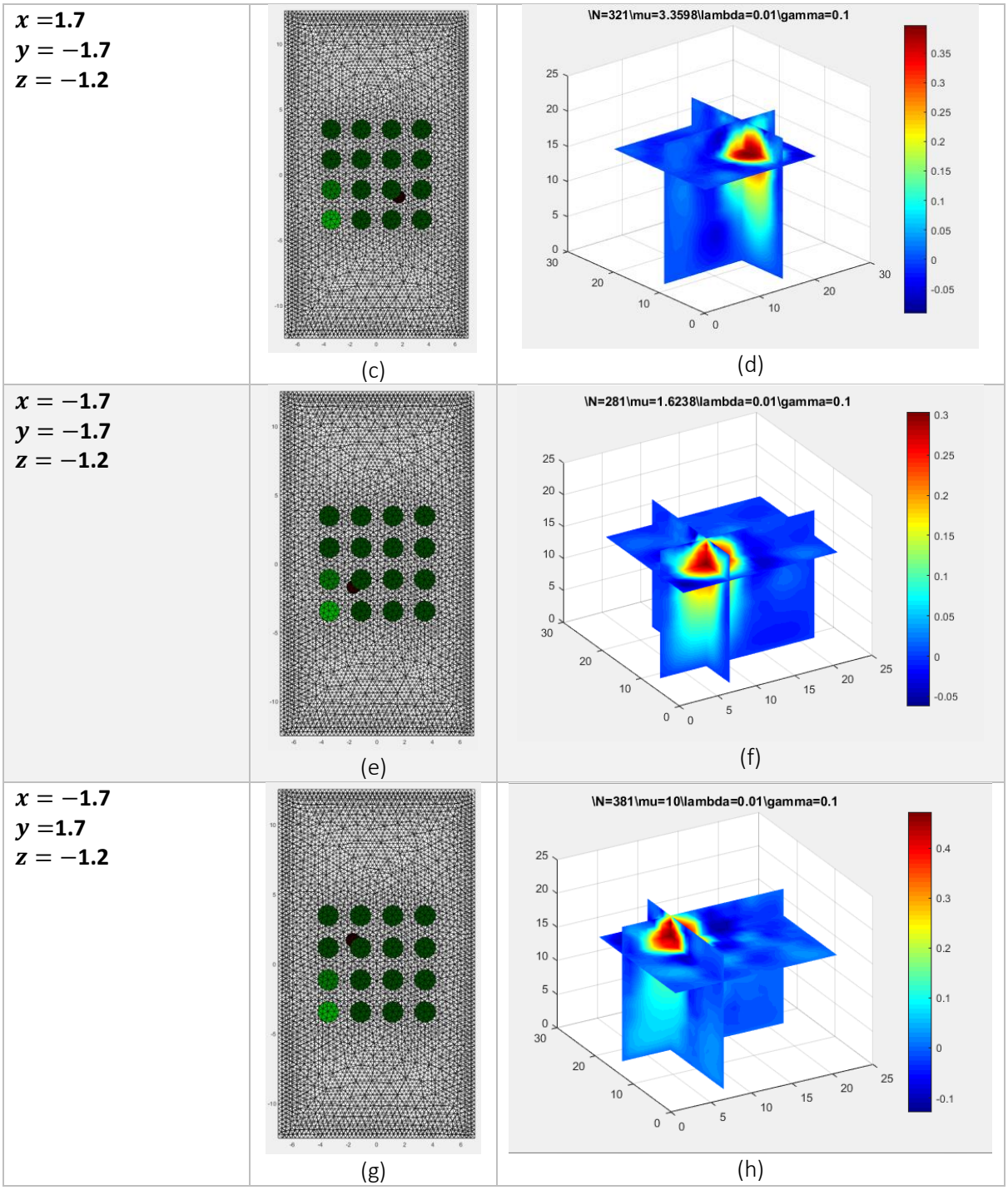

Figure 6.1 Finite element mesh of 4×4 planar array electrode EIT model of 4 positions (a) upper right (c) bottom right (d) bottom left (g) upper left; Reconstructed 3D image of the 4×4 planar array electrode EIT model (b) upper right (d) bottom right (f) bottom left (h) upper left

In the simulation test, the metal ball is detected in the correct position. For the reconstructed images, the colour bar represents the conductivity range. The red area shows the most conductive part within the phantom. The reconstructed images are clear after parameter selection, and the resolution of the images are good.

Simulation test 2

In the simulation test 2, a metal ball with $r = 0.5$ is put on the 4 positions close to the surface of the phantom. And the redundancy analyses are applied to test the quality of the images reconstruction.

Positions	Reconstructed before redundancy analysis	Reconstructed after redundancy analysis	Singular value decomposition(n=96)
x =1.7 y =1.7 z = −1.2	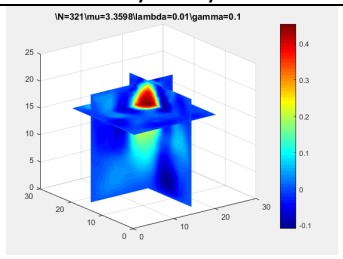 (a)	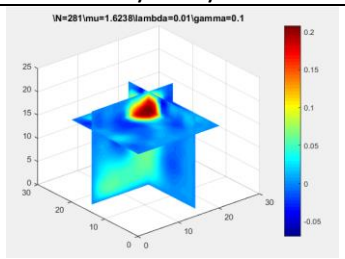 (b)	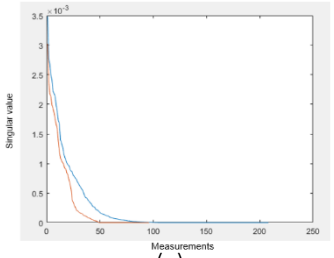 (c)
x =1.7 y = −1.7 z = −1.2	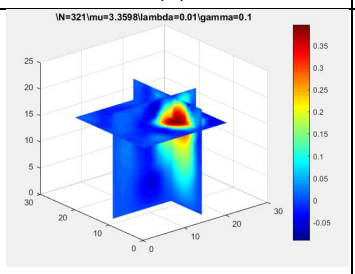 (d)	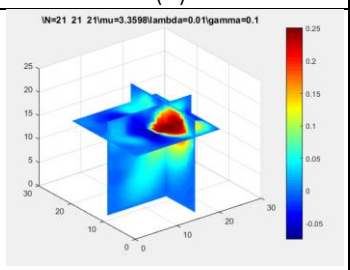 (e)	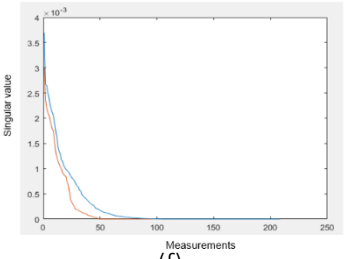 (f)
x = −1.7 y = −1.7 z = −1.2	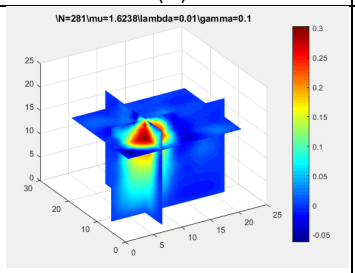 (g)	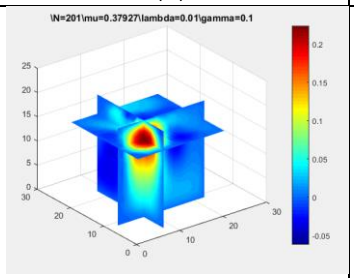 (h)	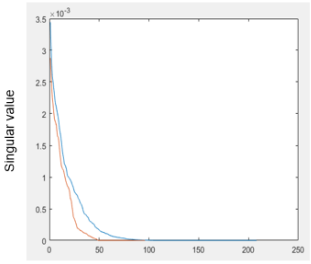 (i)
x = −1.7 y =1.7 z = −1.2	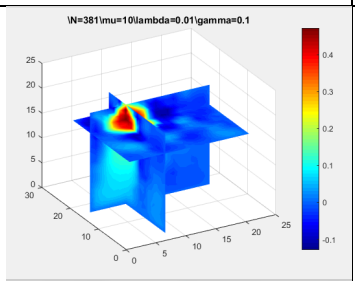 (j)	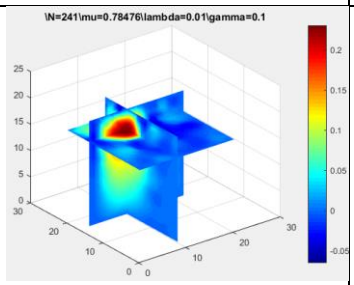 (k)	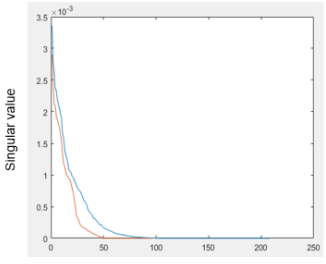 (l)

Figure 6.2 Reconstructed 3D image of the 4×4 planar array electrode EIT model which is before operated redundancy **analyses** (a) upper right (d) bottom right (g) bottom left (j) upper left; Reconstructed 3D images of the 4×4 planar array electrode EIT model which has operated redundancy **analyses** (b) upper right (d) bottom right (h) bottom left (k) upper left; Singular value decomposition. The conductivity distribution data of a total of 208-measurements and valid 96-measurements.

The total measurements of each test is 208. All measured data is divided into valid (96 measurements) and invalid (112 measurements) groups. The metal ball is detected clearly before and after the

redundancy **analyses**, and the quality of reconstructed images is not degraded. It can be seen from the figure (c) (f) (i) (l) that the gap between the singular value of the total 208-measurement conductivity distribution data and that of 96-measurement conductivity distribution data is narrowed considerably.

Simulation test 3

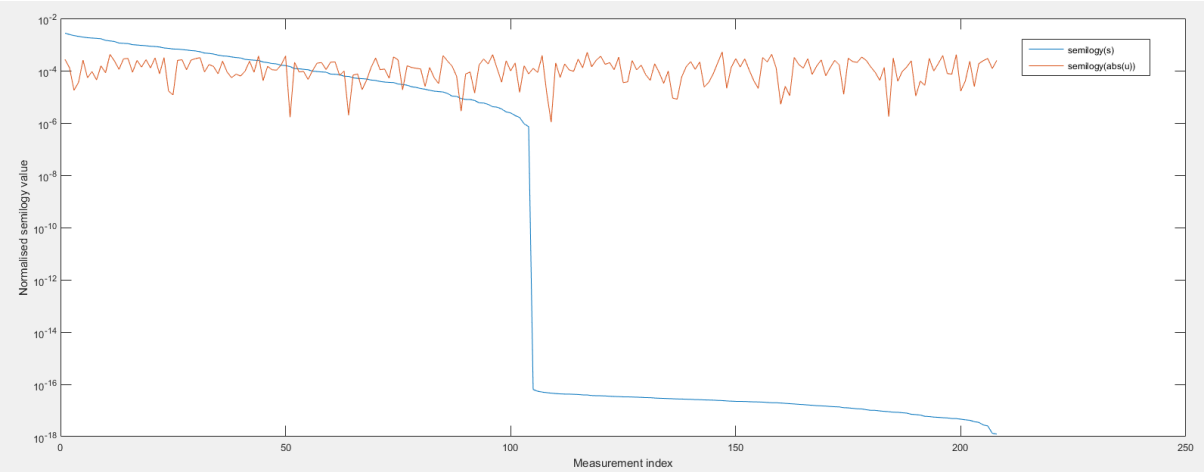

Figure 6.3 L-curve plot

The injection of these two lines are close to the corner of the L-curve which is around number 96. Which means the parameter $\lambda \cong 96$, and it is related to the singular value decomposition. Because when picking up 96 measurements, the quality of reconstructed images is not degraded.

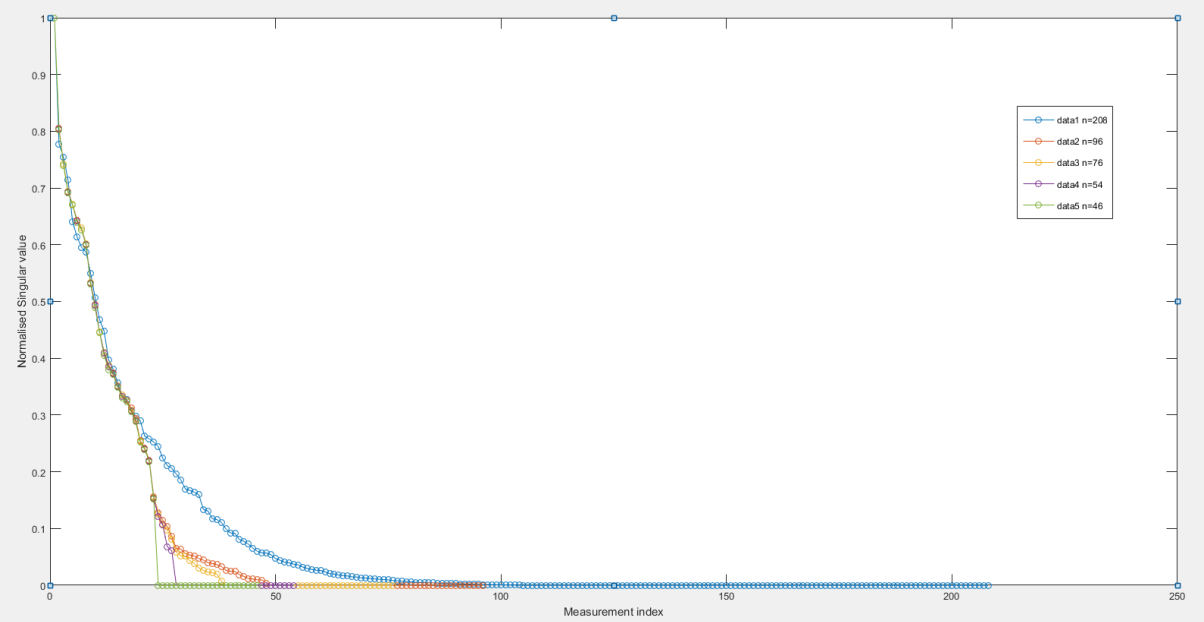

Figure 6.4 Singular value decomposition. The impedance data are divided into 5 groups which are 208 measurements, 96 measurements, 76 measurements, 54 measurements and 46 measurements.

It can be seen from Figure 6.4 that the conductivity distribution data are divided in to 5 groups. The gap between the normalized singular value of 208-measurement impedance data and that of the 96-data is narrowed considerably. The gap is getting wider when the valid measurements is getting smaller. However, the values of the 46-measurement and 54-measurement conductivity distribution decreased immediately when compared to those of the 76-, 96- and 208-measurement conductivity distribution

data. Therefore, useful information might be lost when reconstructing the image when 46-, 54- and 76-measurement are taken.

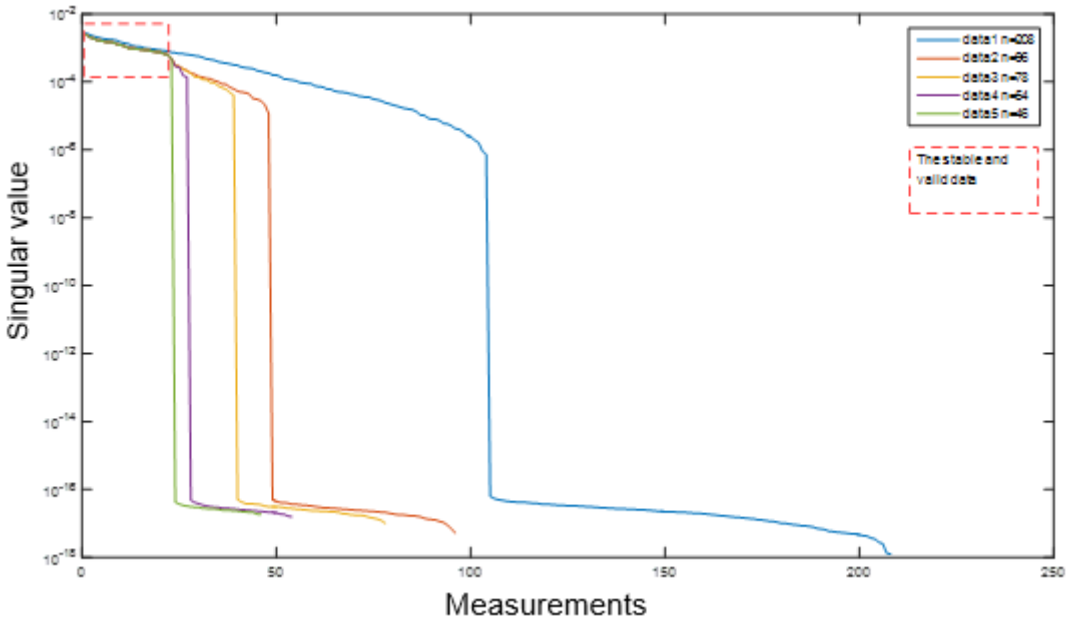

Figure 6.5 Singular value decomposition. Semilogy plot of the impedance data are divided into 5 groups which are 208 measurements, 96 measurements, 76 measurements, 54 measurements and 46 measurements.

It can be seen from the Figure 6.5 that the data within the red rectangle area is stable and reliable, which means that small change would not able to produce big errors in the reconstructed images. Because of the ill-posed problem, SVD regularization is required to improve the quality of the images. And figure 6.5 shows that the different sets of selection of the Jacobian matrix produce different noise levels in the images. The 96-measurement produced better quality images compared to that of the 76-, 54- and 46- measurements, and it saves time and keeps the useful and stable data for image reconstruction.

In the simulation test 3, a metal ball with $r = 0.5$ is put at the center position closed to the surface of the phantom, and the redundancy **analyses** with different n values are applied to test the quality of images reconstruction.

Positions	Reconstructed before redundancy analysis	Reconstructed after redundancy analysis	Singular value decomposition	Reconstructed after redundancy analysis (x direction)
$x = 0$ $y = 0$ $z = -1.2$ N=96	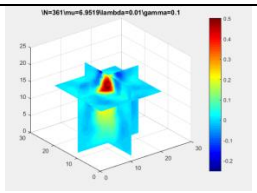 (a)	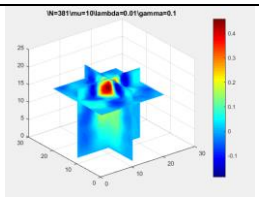 (b)	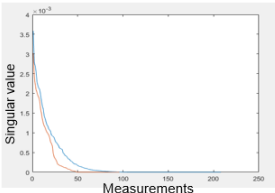 (c)	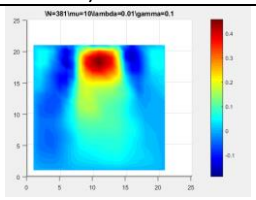 (d)
$x = 0$ $y = 0$ $z = -1.2$ N=76	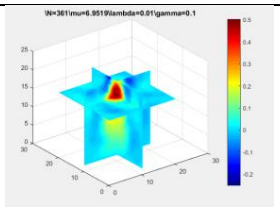 (e)	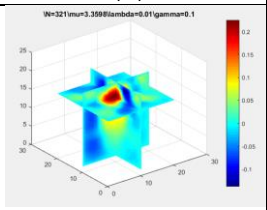 (f)	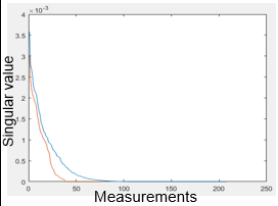 (g)	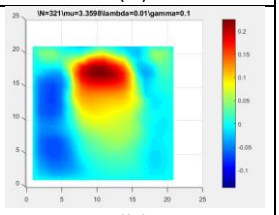 (h)
$x = 0$ $y = 0$ $z = -1.2$ N=54	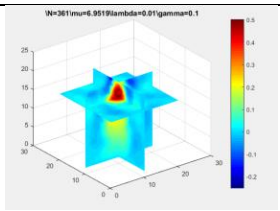 (i)	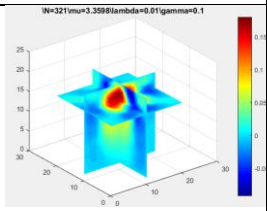 (j)	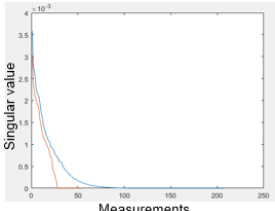 (k)	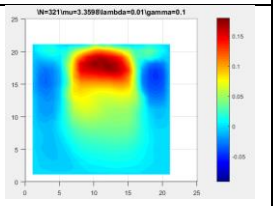 (l)
$x = 0$ $y = 0$ $z = -1.2$ N=46	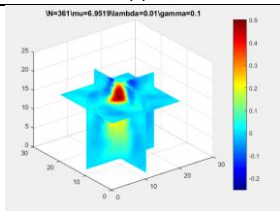 (m)	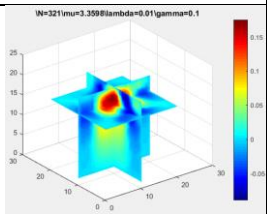 (n)	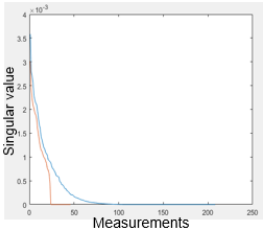 (o)	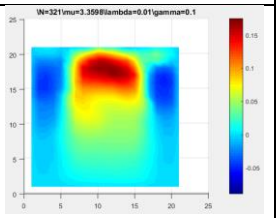 (p)

Figure 6.6 Reconstructed 3D image of the 4×4 planar array electrode EIT model which is before operated redundancy analysis: the metal ball is in the center of the phantom (a)(e)(i)(m); Reconstruction 3D image of the 4×4 planar array electrode EIT model which is operated redundancy **analyses**,: (b) 96-measurement data (f) 76-measurement data (j) 54-measurement data (n) 46-measurement data; Singular value decomposition of (c) 96-measurement data (g) 76-measurement data (k) 54-measurement data (o) 46-measurement data; X-direction of reconstruction 3D image of the 4×4 planar array electrode EIT model which is operated redundancy analysis: (d) 96-measurement data (h) 76-measurement data (l) 54-measurement data (p) 46-measurement data;

It can be seen from Figure 6.6 that the quality of the reconstructed images is getting worse when the number of measurements decreases. The red area of the reconstructed images is getting bigger and the boundary is more blurred. The results show that after the redundancy **analyses**, the reconstructed image using the 96-measurement is as good as that of 208-measurements.

Simulation test 4

In the simulation test 4, a metal ball with $r = 0.5$ is put at the center position closed to the surface of the phantom, and in this test, the metal ball is moving further down at 4 depths. Also the redundancy **analyses** are applied to test the quality of the images reconstruction.

Positions	Reconstructed before redundancy analysis	Reconstructed after redundancy analysis	Singular value decomposition	Reconstructed after redundancy analysis (x direction)
$x = 0$ $y = 0$ $z = -1.2$ N=96	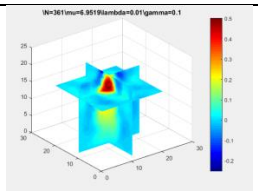 (a)	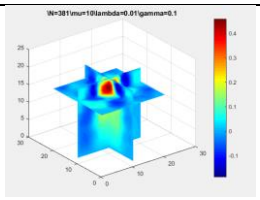 (b)	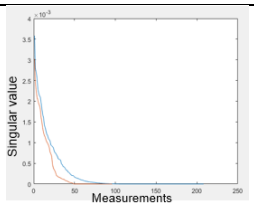 (c)	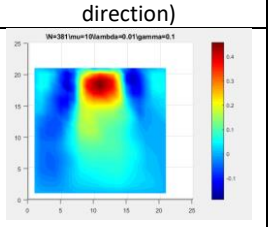 (d)
$x = 0$ $y = 0$ $z = -2.2$ N=96	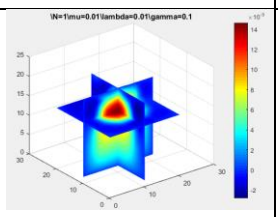 (e)	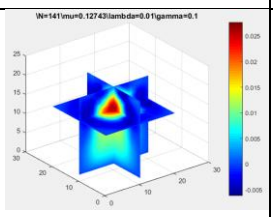 (f)	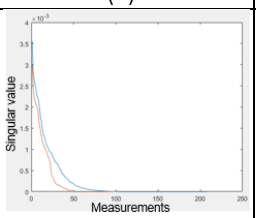 (g)	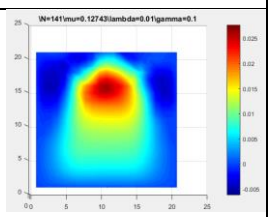 (h)
$x = 0$ $y = 0$ $z = -3.2$ N=96	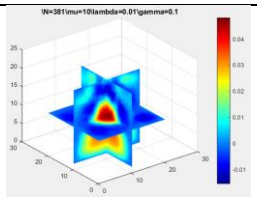 (i)	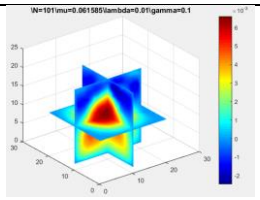 (j)	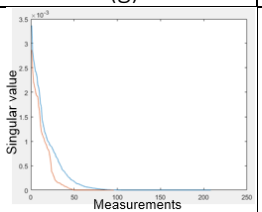 (k)	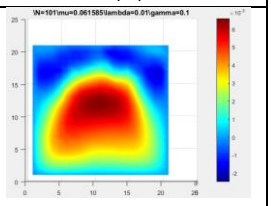 (l)
$x = 0$ $y = 0$ $z = -4.2$ N=96	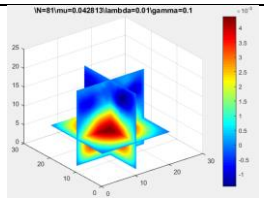 (m)	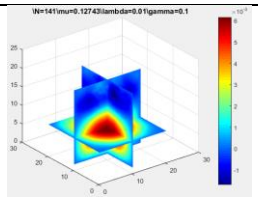 (n)	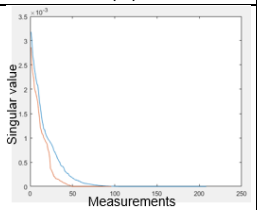 (o)	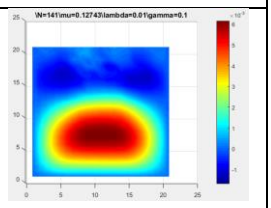 (p)

Figure 6.7 Reconstruction 3D image of the 4×4 planar array electrode EIT model which is before operated redundancy analysis: the metal ball is in the centre of the phantom (a) at depth: -1.2(e) at depth: -2.2 (i) at depth: -3.2 (m) at depth: -4.2; Reconstruction 3D image of the 4×4 planar array electrode EIT model which is after operated redundancy **analyses**: 96-measurement data (b) at depth: -1.2 (f) at depth: -2.2 (j) at depth: -3.2 (n) at depth: -4.2; Singular value decomposition of (c) at depth: -1.2 (g) at depth: -2.2 (k) at depth: -3.2 (o) at depth: -4.2; X-direction of reconstruction 3D image of the 4×4 planar array electrode EIT model which is after operated redundancy **analyses**: (d) at depth: -1.2 (h) at depth: -2.2 (l) at depth: -3.2 (p) at depth: -4.2;

It can be seen from Figure 6.7 that the quality of reconstructed images is getting worse when the depths of detecting objects are increased. The red area of the reconstructed images is getting bigger and the boundary is more blurred. The results show that the conductivity is more sensitive to the surface area by using 3D planar array EIT. And it cannot plot high quality images when the object is far away from the electrode plane.

Conclusion

After the simulation tests, the results show that 3D planar array is best used for detecting the objects which are close to the electrode plane. Also, the quality of reconstructed images is good. Although the image is getting poor when the object is moving down, it is able to clearly detect the position of the object. After redundancy analyses, it is clear that the reconstructed image using the 96-measurements (k-th value) is as good as that of 208-measurements.

Chapter 7: Experimental validation

Phantom design

The phantom is built with width 14cm, length 14cm and height 25cm. It is a cuboid container and there are 4×4 electrodes (circular electrode with radius 7.5cm) on opposite sides of the phantom. 16 electrodes are connected with the KHU Mark 2 acquisition system. Data can be collected and recorded. The frequency is 10kHz when the system is running.

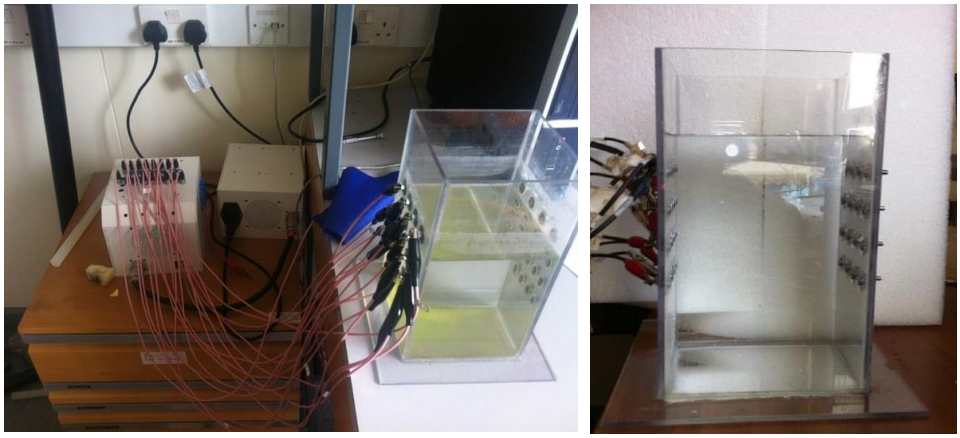

Figure 7.1 3D Planar array phantom

Nowadays most EIT measurement is based on the annulus electrode. For EIT measurement with the annulus electrode, only one image located in the electrode plane can be reconstructed in one measurement, the information obtained is limited. To gain the information of more planes, 3D imaging of EIT using planar array are needed.

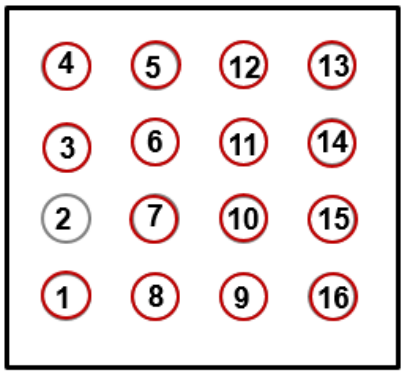

Figure 7.2 The order of electrodes

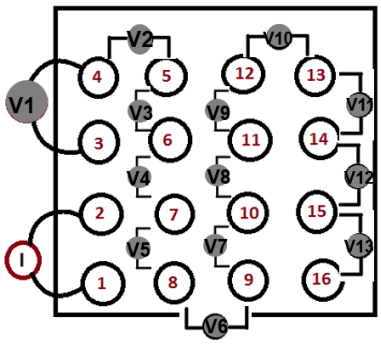

Figure 7.3 Data collection method: *The neighbouring method: Current injection at each of the 16 positions and voltages are measured*;

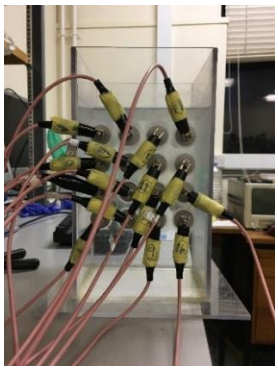

Figure 7.4 The real connection between KHU Mark2 system and phantom.

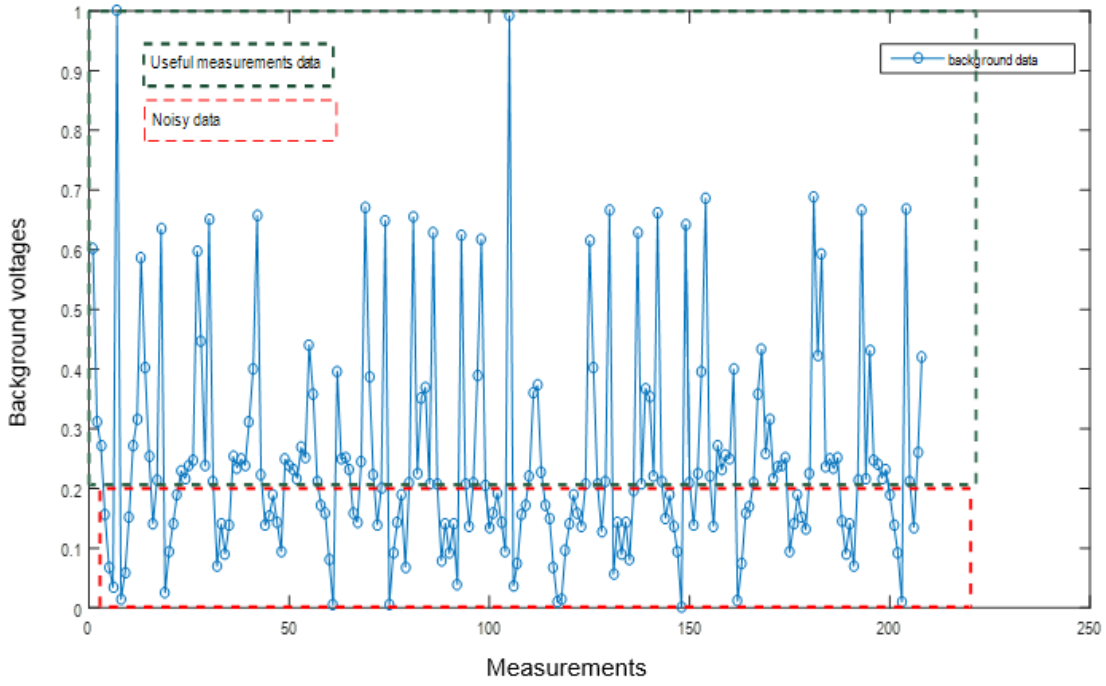

Figure 7.5 Normalized background data of the 3D planar array EIT sensor

The figure shows that the experiments normalized background data. The noise data is below 0.2 which means that the small change of these values will produces a large amount of error for the reconstructed

results. The noise data is the one of the factors which degrades the quality of the reconstructed images. However, the 96-measurements which are in the blue area will produce the similar results and high quality and stable reconstructed images compared with that of the 208-measurements.

Experimental test 1

In the experimental test 1, a metal ball with $r = 1.2$ is put in the center position close to the surface of the phantom. And in this test, the metal ball is moving further down at 4 depths. Also, the results of the simulation test are used to compare the quality of experimental images reconstruction.

Positions	**Reconstructed Simulation images**	**Reconstructed experimental images**
$x = 0$ $y = 0$ $z = -20$	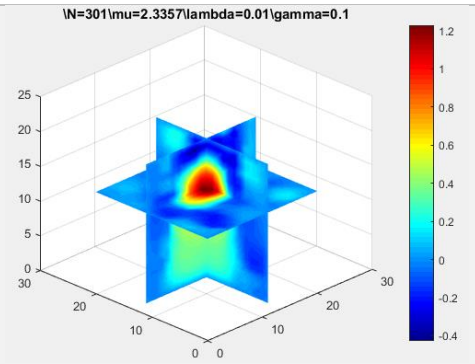 (a)	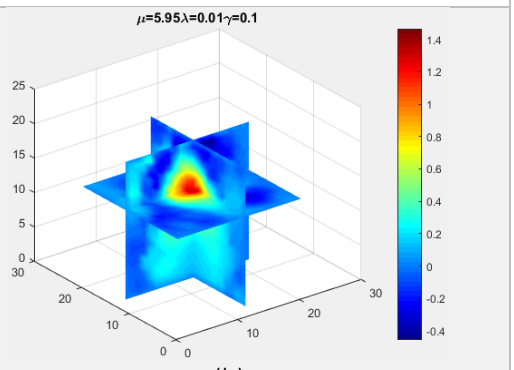 (b)
$x = 0$ $y = 0$ $z = -30$	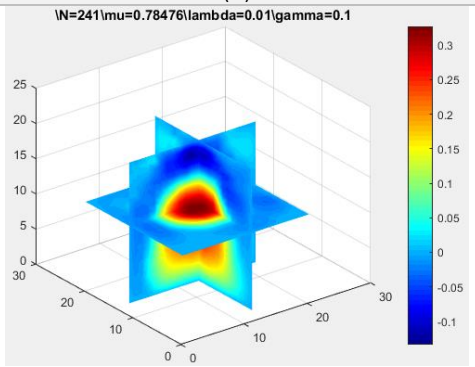 (c)	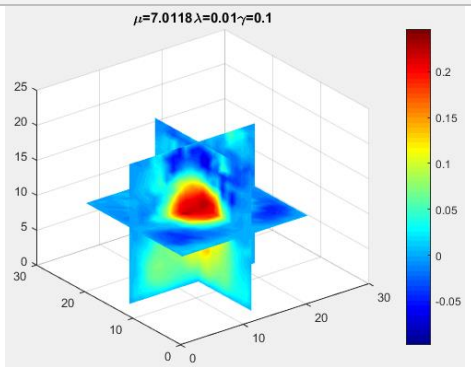 (d)
$x = 0$ $y = 0$ $z = -40$	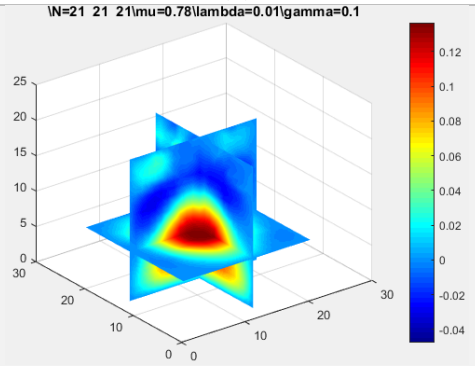 (e)	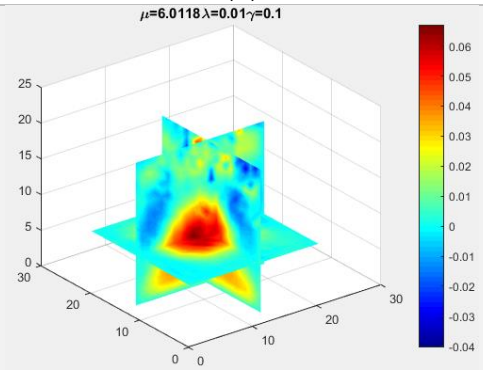 (f)

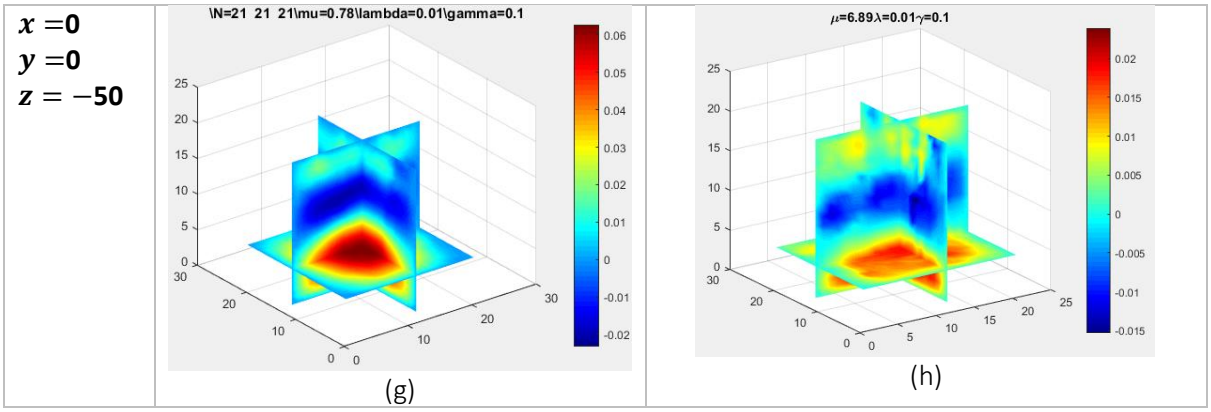

Figure 7.6 Reconstructed 3D simulation images of 4×4 planar array electrode EIT model of 4 positions (a) $\boldsymbol{x}$ =0; $\boldsymbol{y}$ =0; $\boldsymbol{z}$ = −20cm(c) $\boldsymbol{x}$ =0; $\boldsymbol{y}$ =0; $\boldsymbol{z}$ = −30cm (e) $\boldsymbol{x}$ =0; $\boldsymbol{y}$ =0; $\boldsymbol{z}$ = −40cm (g) $\boldsymbol{x}$ =0; $\boldsymbol{y}$ =0; $\boldsymbol{z}$ = −50cm; Reconstructed 3D experimental image of the 4×4 planar array electrode EIT model (b) $\boldsymbol{x}$ =0; $\boldsymbol{y}$ =0; $\boldsymbol{z}$ = −20cm (d) $\boldsymbol{x}$ =0; $\boldsymbol{y}$ =0; $\boldsymbol{z}$ = −30cm (f) $\boldsymbol{x}$ =0; $\boldsymbol{y}$ =0; $\boldsymbol{z}$ = −40cm (h) $\boldsymbol{x}$ =0; $\boldsymbol{y}$ =0; $\boldsymbol{z}$ = −50cm.

In the figure above (a)(c)(e)(g) are 3D simulation images. It is clear that the area of metal is increasing as the depth increases, this is because the distance between the metal ball and electrodes is increasing. In addition, the sensitivity is decreasing and the Noise is increasing. Therefore, the 3D planar array system is able to work within a properly depth between the electrodes and objects.
In the figure (b)(d)(f)(h) are 3D experiment images. When compared to the simulation results, they are more blurred and have less correct detection within the domain.

Here is the assessment between simulation and experimental results below:

Conditions	Simulation results	Experimental results
Signal detection	Strong	Strong
Object detection	YES	YES
Object location	Precisely correct	Less correct
Size and shape reconstruction	Reliable	Less reliable
Reconstruction in depth	Quite accurate	Less accurate

Table 7.1: Reliability assessment of planar array EIT sensor

Experimental test 2

In the experimental test 2, a metal cube with $length\ l = 2.4$ is put in 4 positions close to the surface of the phantom.

Positions		Reconstructed Simulation images	Reconstructed experimental images
x =1.7 y =1.7 z = −20		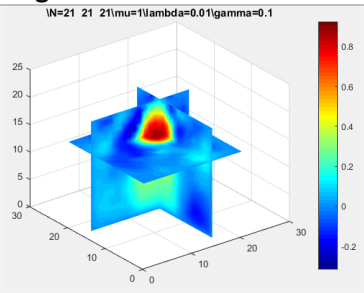 (a)	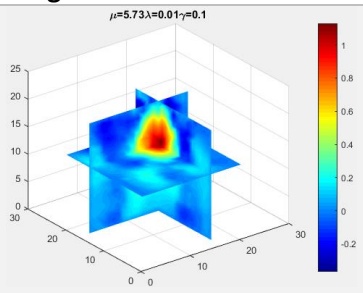 (b)
x =1.7 y = −1.7 z = −20		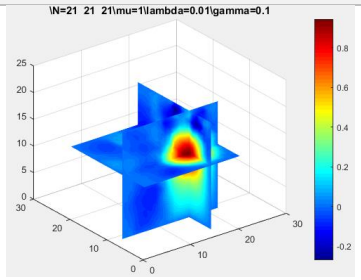 (c)	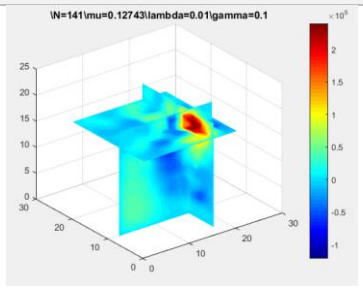 (d)
x = −1.7 y = 1.7 z = −20		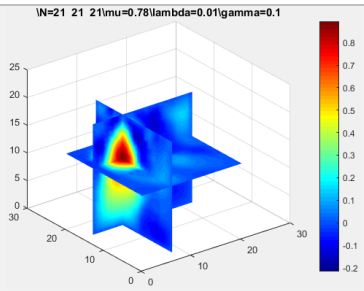 (e)	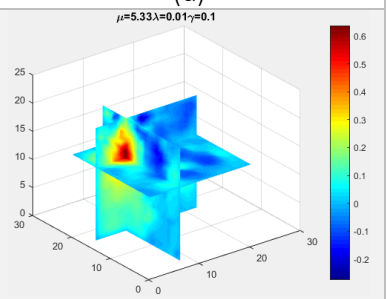 (f)
x =-1.7 y =-1.7 z = −20		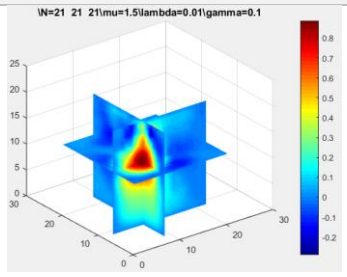 (g)	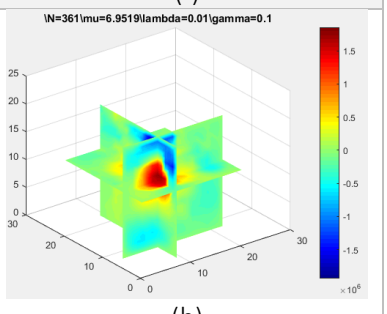 (h)

Figure 7.7 Reconstructed 3D simulation images of the 4×4 planar array electrode EIT model (a) upper right (c) bottom right (e) upper left (g) bottom left; Reconstructed 3D experiment images of the 4×4 planar array electrode EIT model(b) upper right (d) bottom right (f) upper left (h) bottom left. In the Figure (a)(c)(e)(g) are 3D simulation images, and the metal cube is clearly detected. In the figure (b)(d)(f)(h) are 3D experiment images. When compared to the simulation results, they are more blurred and less correct detected within the domain.

Conclusion

In this chapter, two types of experiments are tested to perform and assess the EIT system. Compared to the simulation images, the experimental validation using a real EIT system did not work very well because of the noise and other errors. The object is detected clearly by the real EIT system, however, the quality of reconstructed images is poor. Especially, when the object is moving down, the reconstructed images are bad due to the decreased sensitivity and increasing noises.

Chapter 8: Conclusion and Future work

Conclusion

The aim of this research is to investigate the effective method to reduce errors, effectively raise the measurement sensitivity and improve the resolution of reconstructed 3D EIT Planar array images. The results of simulation and experiment show the achievements of the Mphil course including the solid background knowledge, history, methods and applications of 3D electrical impedance tomography by using Planar array. Also EIT models such as forward model and inverse model are explained in detail. The lab hardware KHU Mark 2 and software EIDORS, Netgen and Matlab are useful tools to run the whole EIT program. The forward model and inverse model of 3D EIT using Planar array are built and are evaluated by using simulation and experiment tests. The total variation and SVD are used to reduce the noise level and improve the quality of reconstructed images.

Future work

The aim of this research is to determine the feasibility to improve the image resolution of 3D planar array EIT. The conductivity distribution data redundancy analysis method for the 3D planar array has been presented and it shows that the data reduction is used to preserve the stability of the image reconstruction process. The work shows the current results of the MPhil course including the solid background knowledge of 3D planar array electrical impedance tomography, mathematical models and algorithms learning. The research is now in the initial development stage and it will be progressed with a good understanding of the EIT systems. The results of improving general image reconstruction problems has been achieved. And the future research is detailed below:

- Further Simulation and Experimental Validation.
- Parameters selection to evaluate the performance, resolution and penetration depth of Planar Electrodes Array based on 3D EIT.
- Specific sensor model development such as a planar array sensor for industry detection or clinic application.
- To improve reconstruction algorithms.
- To construct a 4D/real-time planar array system.

Reference

1. ROSS P. HENDERSON, A.J.G.W., *<An impedance camera for spatially specific measurements of the thorax.pdf>.* IEEE TRANSACTIONS ON BIOMEDICAL ENGINEERING, 1978.
2. Brown, B.H., *Electrical impedance tomography (EIT): a review.* J Med Eng Technol, 2003. **27**(3): p. 97-108.
3. Freeston, C.C.B.B.H.B.I.L., *<Imaging spatial distributions of resistivity using applied potential tomography.pdf>.* Electronics Letters, 1983.
4. Boone, K., D. Barber, and B. Brown, *Imaging with electricity: Report of the European Concerted Action on Impedance Tomography.* Journal of Medical Engineering & Technology, 2009. **21**(6): p. 201-232.
5. Ahsan, S.T., *<Electrical Impedance Tomography (EIT) for brain function imaging.pdf>.* Sci.Int.(Lahore), 2015.
6. Holder, D., *<Electrical Impedance Tomography method and history.pdf>.* Institute of Physics Publishing, 2004.
7. VAUHKONEN, P.J., *<Image Reconstruction in Three-Dimensional Electrical Impedance Tomography.pdf>.* Doctoral dissertation, 2004.
8. Bera, T.K., *Bioelectrical Impedance Methods for Noninvasive Health Monitoring: A Review.* J Med Eng, 2014. **2014**: p. 381251.
9. Zarafshani, A., et al., *Using planar electrical impedance tomography as a structural health monitoring method to detect and evaluate the damage to CFRP composite.* 2016: p. 74-79.
10. Kotre, C.J., *<Subsurface electrical impedance imaging measurement strategy image reconstruction and in vivo results.pdf>.* Physiological Measurement, 1996. **17**.
11. William Lionheart, N.P.a.A.B., *<Electrical Impedance Tomography method and history.pdf>.* December 21, 2004.
12. Wang, J. and B. Han, *Image Reconstruction Based on Homotopy Perturbation Inversion Method for Electrical Impedance Tomography.* Journal of Applied Mathematics, 2013. **2013**: p. 1-11.
13. Erkki Somersalo, M.C., and David Isaacson, *<Existence and Uniqueness for Electrode Models for Electric Current Computed Tomography.pdf>.* Society for Industrial and Applied Mathematics, 1992. **52**.
14. Peimin Yan, S.W., and Luming Shi, *<Electrical Impedance Tomography Based on Sensitivity Theorem with Singular Value Decomposition.pdf>.* Engineering in Medicine and Biology 27th Annual Conference, 2005.
15. Holder, D., *<Electrical Impedance Tomography method and history.pdf>.* Institute of Physics, 2004.
16. Hansen, P.C., *<Regularization tools A matlab package for analysis and solution of discrete illposed problems.pdf>.* 7 October 1992.
17. Santosa, F., *A Backtrojection Algorithm for Electrical Impedance Imaging.* institute of Physical science and technology, 1988.
18. Hu, J., *<Electrical impedance tomography application in breast cancer imaging with deformable boundary.pdf>.* Doctoral dissertation, 2015.
19. Zhou, Z., et al., *Comparison of total variation algorithms for electrical impedance tomography.* Physiol Meas, 2015. **36**(6): p. 1193-209.
20. Lionheart, W.R.B., *EIT reconstruction algorithms: pitfalls, challenges and recent developments.* Physiological Measurement, 2004. **25**(1): p. 125-142.
21. M. Vauhkonen, D.V.a., P. A. Karjalainen, E. Somersalo, and J. P. Kaipio*, *<Tikhonov Regularization and Prior Information in Electrical Impedance Tomography.pdf>.* IEEE TRANSACTIONS ON MEDICAL IMAGING, 1998. **17**.
22. Hansen, P.C., *<The Lcurve and its use in the numerical treatment of inverse problems.pdf>.* SIAM Journal on Applied Mathematics, 1992.

23. HANSEN, P.C., *<Analysis of discrete illposed problems by means of the lcurve.pdf>.* SIAM Journal on Applied Mathematics, 1992. **34**.
24. HANSENt, P.C., *<Analysis of discrete illposed problems by means of the lcurve.pdf>.* Society for Industrial and Applied Mathematics, 1992.
25. A. Borsic, B.M.G., A. Adler, W. R. B. Lionheart, *<In vivo impedance imaging with total variation regularization.pdf>.*
26. Borsic, A.a.G., Brad M. and Adler Andy and Lionheart, William R.B., *Total Variation Regularization in Electrical Impedance Tomography.*
27. Adler1, A., et al., *<GREIT a unified approach to 2D linear EIT reconstruction of lung images.pdf>.* 2009.
28. Kim, D.Y., et al., *Performance evaluation of KHU Mark2 parallel multi-frequency EIT system.* Journal of Physics: Conference Series, 2010. **224**: p. 012013.
29. al, M.V.e., *<a matlab package for EIT projects.pdf>.* Physiol., 2002: p. Meas. 22 107.
30. A J Wilson, P.M., A R Waterworth, R H Smallwood and B H Brown, *<MK3.5 a modular multifrequency successor to the MK3A EISEIT SYSTEM.pdf>.* Physiol. , 2000. **Meas.** (22 (2001)): p. 49–54
31. Oh, T.I., et al., *A fully parallel multi-frequency EIT system with flexible electrode configuration: KHU Mark2.* Physiol Meas, 2011. **32**(7): p. 835-49.
32. Oh, T.I., et al., *Validation of a multi-frequency electrical impedance tomography (mfEIT) system KHU Mark1: impedance spectroscopy and time-difference imaging.* Physiol Meas, 2008. **29**(3): p. 295-307.
33. Oh, T.I., et al., *Calibration methods for a multi-channel multi-frequency EIT system.* Physiol Meas, 2007. **28**(10): p. 1175-88.
34. Oh, T.I., E.J. Woo, and D. Holder, *Multi-frequency EIT system with radially symmetric architecture: KHU Mark1.* Physiol Meas, 2007. **28**(7): p. S183-96.
35. Qingsheng Zhu, W.R.B., Lionheart, F. John Lidgey, Christopher N. McLeod, Kevin S. Paulson, and Michael K. Pidcock *<An adaptive current tomograph using voltage sources.pdf>.* IEEE TRANSACTIONS ON BIOMEDICAL ENGINEERING., 1993. **40**: p. 2.
36. C.N.McLeod, F.J.L.a.Q.S.Z., *<Multiple drive EIT systems.pdf>.*
37. Q S Zhu, C.N.M., C W Denyer, F J Lidgey and W R B Lionheart, *<Development of a real time adaptive current tomograph.pdf>.* Physiol. Mens., 1994: p. A37-A43.
38. Lionheart, N.P.a.W.R.B., *A Matlab toolkit for three-dimensional electrical impedance tomography: a contribution to the Electrical Impedance and Diffuse Optical Reconstruction Software project.* Measurement Science and Technology, 2002. **13**: p. 1871.
39. Lionheart, N.P.a.W.R.B., *<A Matlab toolkit for three-dimensional electrical impedance tomography.pdf>.* Meas. Sci., 2002: p. Technol. 13 1871.
40. M Vauhkonen1, W.R.B.L., L M Heikkinen1, P J Vauhkonen1 and a.J.P. Kaipio1, *<a matlab package for EIT projects.pdf>.* INSTITUTE OF PHYSICS PUBLISHING, 2000.
41. VAVASISz, S.A.M.A.S.A., *<Quality mesh generation in higher dimensions.pdf>.* Society for Industrial and Applied Mathematics, 2000.
42. Sch¨oberl?, J., *<Netgen An advancing front 2D and 3D-mesh generator based on abstract rules.pdf>.* Computing and Visualization in Science, 1997.
43. Sadosa, F., *<A backprojection algorithm for electrical impedance imaging.pdf>.* Institute for physical science and technology, 1988.
44. COMSOL, *FEMLAB: Refence Manua.* 1999.
45. Adler, A. and W.R. Lionheart, *Uses and abuses of EIDORS: an extensible software base for EIT.* Physiol Meas, 2006. **27**(5): p. S25-42.
46. Stefano Pisa, E.P., and Emanuele Piuzzi *<Comparisons among EIT data collection techniques and reconstruction algorithms.pdf>.* Applied Computational Electromagnetics Society Journal, 2017.

47. Cherepenin, V., et al., *A 3D electrical impedance tomography (EIT) system for breast cancer detection.* Physiological Measurement, 2001. **22**(1): p. 9-18.